




TRIM69 Inhibits Vesicular Stomatitis Indiana Virus

Suzannah J. Rihn,^a Muhamad Afiq Aziz,^a Douglas G. Stewart,^a Joseph Hughes,^a Matthew L. Turnbull,^a Mariana Varela,^a Elena Sugrue,^a Christie S. Herd,^a Megan Stanifer,^b Steven P. Sinkins,^a Massimo Palmarini,^a  Sam J. Wilson^a

^aMRC-University of Glasgow Centre for Virus Research, Glasgow, United Kingdom

^bDepartment of Infectious Diseases, Virology, Heidelberg University Hospital, Heidelberg, Germany

ABSTRACT Vesicular stomatitis Indiana virus (VSIV), formerly known as vesicular stomatitis virus (VSV) Indiana (VSV_{IND}), is a model virus that is exceptionally sensitive to the inhibitory action of interferons (IFNs). Interferons induce an antiviral state by stimulating the expression of hundreds of interferon-stimulated genes (ISGs). These ISGs can constrain viral replication, limit tissue tropism, reduce pathogenicity, and inhibit viral transmission. Since VSIV is used as a backbone for multiple oncolytic and vaccine strategies, understanding how ISGs restrict VSIV not only helps in understanding VSIV-induced pathogenesis but also helps us evaluate and understand the safety and efficacy of VSIV-based therapies. Thus, there is a need to identify and characterize the ISGs that possess anti-VSIV activity. Using arrayed ISG expression screening, we identified TRIM69 as an ISG that potently inhibits VSIV. This inhibition was highly specific as multiple viruses, including influenza A virus, HIV-1, Rift Valley fever virus, and dengue virus, were unaffected by TRIM69. Indeed, just one amino acid substitution in VSIV can govern sensitivity/resistance to TRIM69. Furthermore, TRIM69 is highly divergent in human populations and exhibits signatures of positive selection that are consistent with this gene playing a key role in antiviral immunity. We propose that TRIM69 is an IFN-induced inhibitor of VSIV and speculate that TRIM69 could be important in limiting VSIV pathogenesis and might influence the specificity and/or efficacy of vesiculovirus-based therapies.

IMPORTANCE Vesicular stomatitis Indiana virus (VSIV) is a veterinary pathogen that is also used as a backbone for many oncolytic and vaccine strategies. In natural and therapeutic settings, viral infections like VSIV are sensed by the host, and as a result the host cells make proteins that can protect them from viruses. In the case of VSIV, these antiviral proteins constrain viral replication and protect most healthy tissues from virus infection. In order to understand how VSIV causes disease and how healthy tissues are protected from VSIV-based therapies, it is crucial that we identify the proteins that inhibit VSIV. Here, we show that TRIM69 is an antiviral defense that can potently and specifically block VSIV infection.

KEYWORDS ISG, interferon, restriction, TRIM69

Most invading pathogens are sensed by the vertebrate host, ensuring that immune defenses are appropriately deployed. Following sensing, a common outcome is the secretion of type I interferons (IFNs) whose signaling results in the upregulation of hundreds of IFN-stimulated genes (ISGs) (1, 2). Many ISG products interfere with viruses directly, generating an antiviral state in stimulated cells that impedes the infection, replication, or propagation of viruses (3–5). In addition, many ISGs are themselves involved in pathogen sensing and signal transduction, placing cells in a heightened state of alert whereby they are poised to detect invading pathogens (6). The IFN response typically involves hundreds of ISGs, many of which have been regulated by IFNs for hundreds of millions of years (1). Although the major role that IFNs play in

Citation Rihn SJ, Aziz MA, Stewart DG, Hughes J, Turnbull ML, Varela M, Sugrue E, Herd CS, Stanifer M, Sinkins SP, Palmarini M, Wilson SJ. 2019. TRIM69 inhibits vesicular stomatitis Indiana virus. *J Virol* 93:e00951-19. <https://doi.org/10.1128/JVI.00951-19>.

Editor Stacey Schultz-Cherry, St. Jude Children's Research Hospital

Copyright © 2019 Rihn et al. This is an open-access article distributed under the terms of the [Creative Commons Attribution 4.0 International license](https://creativecommons.org/licenses/by/4.0/).

Address correspondence to Sam J. Wilson, Sam.Wilson@glasgow.ac.uk.

S.J.R., M.A.A., and D.G.S. contributed equally to this work.

Received 12 June 2019

Accepted 24 July 2019

Accepted manuscript posted online 2 August 2019

Published 30 September 2019

constraining viral pathogenesis and viral colonization is well established, because IFN responses involve so many ISGs, it is often unclear which individual gene products inhibit a given virus.

Vesicular stomatitis Indiana virus (VSIV) is a virus that is mainly restricted to the Americas, where it causes vesicular stomatitis, a disease that primarily affects ungulates, and also rarely causes mild infections in humans (7–9). VSIV is transmitted by biting insects and causes characteristic vesicular lesions at bite sites around the hooves, mouth, nose, teats, and coronary bands (7). Although complications can occur, natural VSIV infection is typically mild and rapidly resolved. In contrast, experimental VSIV infection can be highly pathogenic and neurotropic in young mice (10).

In addition to being a notable veterinary pathogen, VSIV has been used extensively as a model virus and has been integral to our understanding of vesiculovirus and rhabdovirus biology. Notably, vesiculoviruses can be particularly sensitive to IFNs, leading to their inclusion in the IFN unit definition assay (11). Indeed, type I IFNs likely play a major role in limiting the severity of VSIV infections, and multiple ISGs have been ascribed anti-VSV activity (4, 12–15).

Importantly, IFNs play a major role in constraining VSIV *in vivo*. Type I IFN receptor (IFNAR) knockout (KO) mice succumb to doses of VSIV that are several orders of magnitude lower than a lethal dose in wild-type (WT) mice (16). Moreover, while VSIV is largely restricted to the central nervous system (CNS) in lethally infected WT mice, VSIV colonizes multiple organs in IFNAR KO mice (16). Interestingly, it is likely that multiple ISGs are involved in limiting the tissue tropism of VSIV. Specifically, it appears that IFIT2 is crucial for preventing VSIV colonization of the brain, but it is not solely responsible for limiting VSIV replication in other organs (15). Thus, other ISGs must play key roles in limiting VSIV tissue tropism. Importantly, VSIV causes neurological disease in multiple species following intracranial inoculation (17, 18), suggesting that the ability of ISGs to prevent VSIV from initially accessing the CNS is the cornerstone in limiting VSIV neuropathology across multiple species (19).

VSIV's low pathogenicity in humans, its rapid replication, and ease of genetic manipulation have made this virus the basis of multiple therapeutic strategies. For example, VSIV can be modified to express antigens from heterologous viruses that can be utilized as vaccine strategies (20). This approach has achieved recent notable success in conferring protection from Ebola virus infection (21). Similarly, VSIV has been used as the backbone of multiple oncolytic strategies (22). Just as with natural VSIV infection, IFNs and ISGs appear to be critical for preventing oncolytic viruses from invading healthy tissues (23, 24) and could be critical determinants governing whether oncolytic vesiculoviruses will be efficacious (25). Furthermore, ISGs likely play a key role in limiting the replication of VSIV-based vaccines and are an important safety feature of this immunization strategy.

The key roles that ISGs play in constraining VSIV pathogenesis and limiting VSIV replication (in natural infection, oncolytic therapies, and vaccine strategies) mean that there is a need to better understand both how and which ISGs inhibit VSIV. Using arrayed ISG expression screening, we identified the anti-VSIV activity of TRIM69, a relatively poorly characterized TRIM protein. Through exogenous expression and CRISPR/Cas9 knockout, we demonstrate that both exogenous and endogenous TRIM69 have potent anti-VSIV activity. Importantly, the inhibition is highly specific for VSIV as multiple other viruses were not inhibited by TRIM69. Notably, TRIM69 shows strong signatures of positive selection, and multiple common alleles circulate in human populations. Interestingly, murine orthologues of TRIM69 had no detectable anti-VSIV activity whereas rat TRIM69 possessed potent antiviral activity. We speculate that TRIM69 could be an important ISG for protecting healthy tissues from VSIV and might therefore limit VSIV pathogenesis and influence the specificity and efficacy of vesiculovirus-based therapeutic strategies.

(This article was submitted to an online preprint archive [26]).

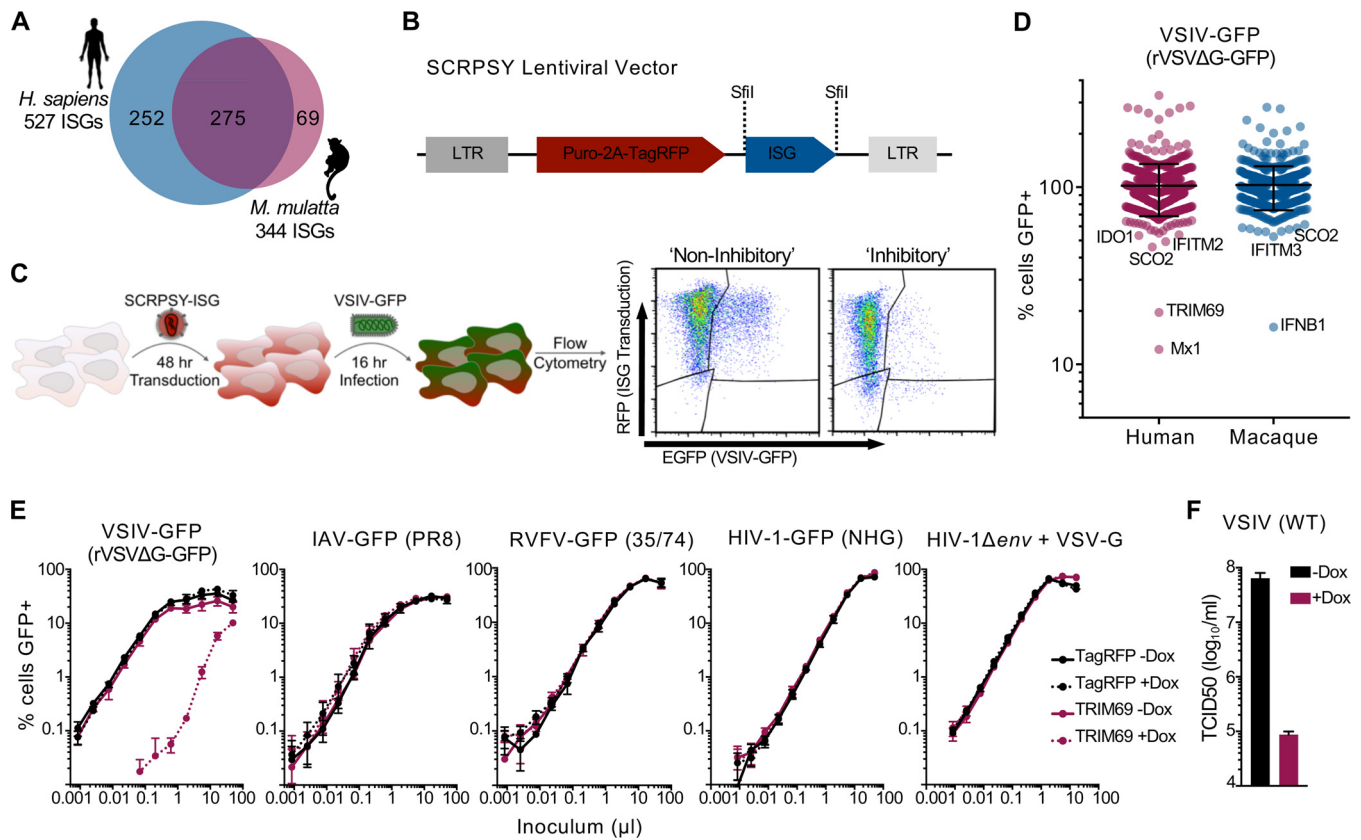


FIG 1 Arrayed ISG expression screening reveals the potent anti-VSIV activity of TRIM69. (A) A schematic of the ISG libraries used herein. (B) A schematic of the SCRPSY lentiviral vector (GenBank accession no. [KT368137.1](#)) used to deliver ISGs shown in panels C and D (one ISG per well of a 96-well plate). (C) A schematic of the ISG screening pipeline used in panel D. (D) Normalized infection (median centered) of cells expressing different ISGs (each dot represents the observed infection in the presence of a single ISG). The screen was executed once. (E) MT4 cells (modified to express doxycycline-inducible TRIM69) were incubated with and without doxycycline for 24 h and then challenged with serially diluted GFP-encoding variants of VSIV for 16 h, influenza A virus (IAV) for 16 h, RVFV (Rift Valley fever phlebovirus) for 48 h, or HIV-1 for 48 h prior to fixation and enumeration of GFP-positive cells using flow cytometry. Virus titrations were carried out on at least two occasions, and typical results are shown. Mean values of experimental replicates are plotted, and error bars represent standard deviations. (F) The same cells as used for the experiment shown in panel E were infected with unmodified (WT) VSIV, and infectivity/replication was quantified using TCID₅₀. The mean and standard deviation are plotted. Dox, doxycycline.

RESULTS

ISG expression screening reveals the anti-VSIV activity of TRIM69. We have previously used arrayed ISG expression screening of human and rhesus macaque ISG libraries to identify antiviral factors targeting a range of viruses (3, 5, 27). Although VSIV has previously been subjected to a large-scale screen of ~300 ISGs (4), we reasoned that using larger libraries of arrayed ISGs might identify additional anti-VSIV effectors. We recently expanded our human ISG library to include >500 ISGs, which can be used in conjunction with our existing library of >300 rhesus macaque ISGs (5, 27) (Fig. 1A), all of which are encoded by lentiviral vectors (Fig. 1B). In addition, we took advantage of a single-cycle VSIV-green fluorescent protein (VSIV-GFP) system (recombinant vesicular stomatitis virus where the glycoprotein [G] has been deleted and replaced with GFP [rVSVΔG-GFP], referred to herein as VSIV-GFP) to allow us to identify strong early blocks to VSIV with high fidelity (28). We first transduced human MT4 cells with each ISG-encoding lentiviral vector and then challenged these cells with VSIV-GFP, using a dose whereby ~30% of cells were infected (Fig. 1C). The level of VSIV-GFP infection in the presence of each individual ISG was then quantified using flow cytometry (Fig. 1C and D). Strikingly, only three genes potently inhibited VSIV under these conditions: macaque IFNB1, human Mx1, and human TRIM69. Although we identified only one ortholog of each gene, we do not ascribe this to species-specific antiviral activity as macaque TRIM69 and human IFNB1 were not present in these libraries. Moreover, the

isoform of macaque Mx1 included in the screen lacked 154 N-terminal residues relative to the sequence of the human counterpart (that exhibited anti-VSIV activity), potentially explaining the lack of inhibition conferred by the macaque variant. Importantly, TRIM69 was not identified in the previous ISG screen of VSIV as it was not present in the ISG library used (4).

TRIM69 exhibits potent and highly specific antiviral activity. Because the anti-VSIV activities of type I IFN and Mx1 are well documented (13, 16), we were immediately struck by how potent the TRIM69-mediated inhibition of VSIV was in our initial screen (Fig. 1D). At the time that these experiments were carried out, TRIM69 had not been ascribed any antiviral activity, so we examined the ability of doxycycline-inducible TRIM69 to inhibit a small panel of viruses. Notably, while VSIV-GFP infection was reduced by >100-fold by TRIM69, the other viruses in our panel [influenza A virus A/Puerto Rico/8/1934 (H1N1) (PR8), Rift Valley fever phlebovirus (RVFV 35/74), and HIV-1 (NHG)] were unaffected by TRIM69 expression (Fig. 1E). It is well documented that many TRIM proteins are involved in antiviral signaling, which can often be triggered by exogenous expression (5, 29–31). Moreover, exogenous or endogenous expression of many ISGs can promote cell death (32). However, the highly specific antiviral activity of TRIM69 against VSIV suggests that the antiviral mechanism does not involve global processes such as cellular toxicity or the induction of a polygenic antiviral state. Interestingly, a VSV-G (glycoprotein) pseudotyped variant of HIV-1 that does not express an HIV-1 envelope glycoprotein and was decorated with a VSV-G envelope derived from VSIV was also insensitive to TRIM69-mediated inhibition (Fig. 1E). This suggests that inhibition of VSIV by TRIM69 occurs after viral entry and that the VSIV glycoprotein is not directly targeted by TRIM69. Importantly, unmodified wild-type replication-competent VSIV was also potently inhibited by TRIM69 (Fig. 1F).

Endogenous TRIM69 is IFN inducible and potently inhibits VSIV. We have previously used comparative transcriptomics to study the IFN response in a variety of species (1). Meta-analysis of these data indicated that TRIM69 expression was upregulated ~10-fold following IFN stimulation in primary human fibroblasts (Fig. 2A). Similarly, TRIM69 has been previously identified as an ISG in multiple studies and is typically induced between ~2- and ~10-fold by type I IFNs (2, 33). To examine whether the endogenous protein exhibited antiviral activity, we knocked out TRIM69 using CRISPR/Cas9 in diploid CADO-ES1 cells (34). We selected CADO-ES1 cells for these experiments as existing transcriptomics data suggested that TRIM69 was efficiently expressed in these cells (EMBL-EBI Expression Atlas [<https://www.ebi.ac.uk/gxa/home>]). TRIM69 knock-out (KO) single-cell clones were derived, and the KO was confirmed by sequencing the genetic lesions. In accordance with the IFN-sensitive nature of vesiculoviruses, IFN treatment potently blocked VSIV infection in “no-guide” control clones (by >10,000-fold) (Fig. 2B and D). In striking contrast, when TRIM69 was knocked out, the protective effect of IFN was markedly reduced (by ~300-fold). This indicates that endogenous TRIM69 appears to play a major role in the anti-VSIV effects of IFN. Furthermore, the TRIM69 anti-VSIV activity was again specific as the magnitude of HIV-1 inhibition was largely similar in the presence or absence of TRIM69 (Fig. 2C and E). Because CADO-ES1 cells do not support efficient HIV-1 infection, a pseudotyped HIV-1-based lentiviral vector (CSGW) was used for these experiments.

Not all TRIM69 isoforms confer antiviral activity. Because alternative splicing can produce divergent variants of antiviral factors, these spliced isoforms can exhibit differential antiviral activity. In the case of another TRIM protein, TRIM5, the spliced isoforms have been informative in understanding the mechanism of TRIM5's antiviral activity (35). We therefore considered whether all isoforms of TRIM69 conferred anti-VSIV activity. We cloned the five human TRIM69 isoforms listed on ENSEMBL, and we considered their activity in our doxycycline-inducible system. Using this strategy, we were able to detect expression of only isoforms A and B by Western blotting (Fig. 3A) even though the polyclonal antibody should recognize all isoforms. The only variant that conferred anti-VSIV activity was the longest isoform, isoform A (Fig. 3B to D), which

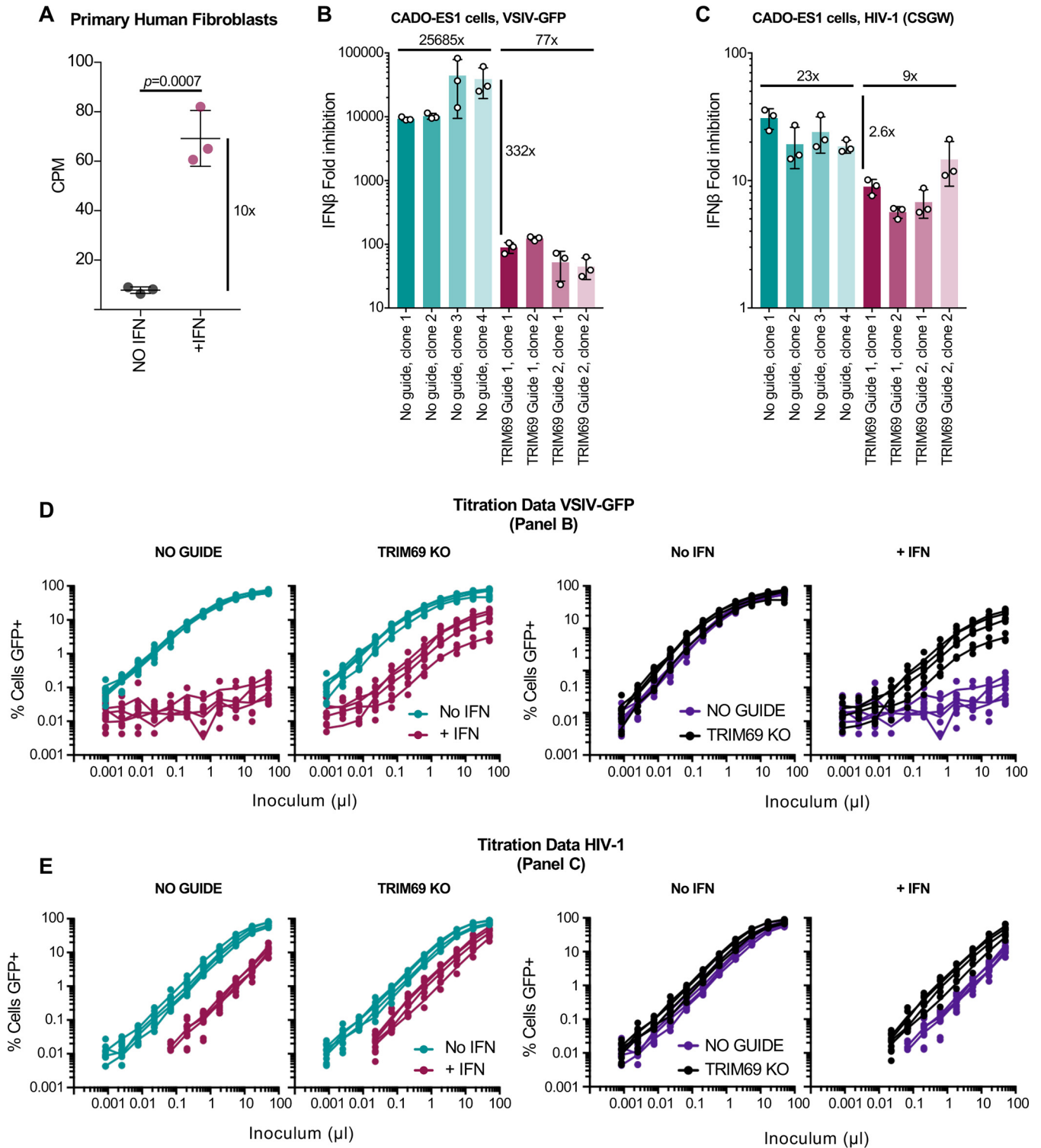


FIG 2 IFN-stimulated endogenous TRIM69 has potent anti-VSIV activity. (A) TRIM69 expression in primary human fibroblasts following 4 h in the presence or absence of 1,000 units/ml of universal IFN. The transcriptomes were defined using transcriptome sequencing (RNA-seq) (1), and the meta-analyzed TRIM69 expression in counts per million (CPM) is plotted. (B) VSIV-GFP inhibition was measured in CADO-ES1 cells in which TRIM69 expression was knocked out using CRISPR/CAS9 or in CADO-ES1 cells that were transduced with no-guide controls. Titrated challenges were used to determine the titer, at 16 h postinfection, in the presence and absence of IFN stimulation and to correspondingly calculate the fold inhibition. Fold inhibition was calculated from three experiments; each experiment is represented by the circles (each circle displays a mean of fold inhibition calculated from three titration points in the linear range), and the mean and standard deviation are plotted. The fold rescue in inhibition (332x) is indicated by the vertical line. (C) The experiment was performed as described for panel B using a single-cycle HIV-1 reporter system (CSGW) (65). (D) The VSIV-GFP titration data (each curve represents an individual clone) in the presence and absence of IFN treatment, as described for panel B, are presented. (E) As described for panel D, the HIV-1 (CSGW) titration data from panel C are shown.

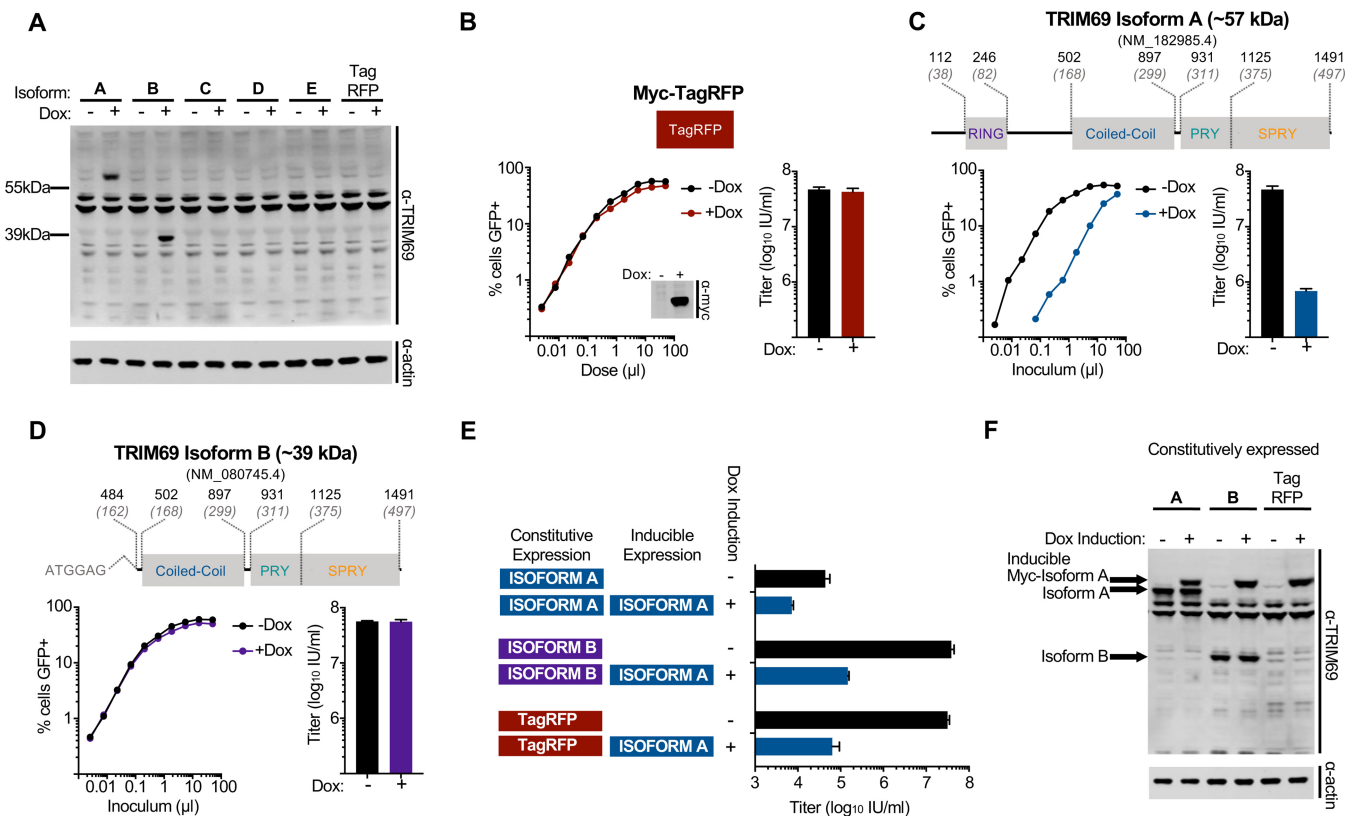


FIG 3 TRIM69 isoform A, but not isoform B, restricts VSIV. (A) Western blot analysis of TRIM69 expression (isoforms A to E) using a polyclonal anti-TRIM69 antibody (PA5-12215 [ThermoFisher], raised against TRIM69 residues 336 to 365, which are present in all isoforms). (B) MT4 cells were modified to express Myc-TagRFP (where RFP is red fluorescent protein) in a doxycycline-inducible fashion. An illustration of TagRFP is depicted above typical titration curves of VSIV-GFP, the VSIV-GFP titers (16 h postinfection), and Western blot analysis of Myc-TagRFP expression (24 h postinduction) in the presence and absence of doxycycline treatment. (C) MT4 cells were modified to express myc-TRIM69 isoform A in a doxycycline-inducible fashion. An illustration of TRIM69 isoform A (predicted mass, ~57 kDa) is depicted above typical titration curves of VSIV-GFP and the VSIV-GFP titers of inducible TRIM69 isoform A expression in the presence and absence of doxycycline treatment. (D) Data are as described in panel C but for isoform B (predicted mass, ~39 kDa). (E) Cells described in the legend of panel C were modified to constitutively express TRIM69 isoform A, isoform B, or TagRFP (by LHCX transduction). The titer of VSIV-GFP was determined in the presence and absence of doxycycline-inducible myc-TRIM69 isoform A. (F) Western blot analysis of the cells used in the experiment shown in panel E. In all cases, virus titrations were carried out on at least two occasions, and typical results are shown. Mean titers and standard deviations are plotted based on at least three doses (in the linear range).

potently inhibited VSIV-GFP infection. Notably, isoform B was abundantly expressed (Fig. 3A), and we thus concluded that this isoform has no anti-VSIV activity. This suggests that the RING domain (or flanking sequence) is critically required for anti-VSIV activity or the correct folding or multimerization of TRIM69. Although we were unable to express or detect isoforms C, D, and E, because these isoforms also lack the N-terminal residues missing in isoform B, we find it unlikely that they possess anti-VSIV activity.

As well as lacking antiviral activity, shorter isoforms of the TRIM5 protein can form heteromultimers with TRIM5α and act as dominant negative inhibitors of endogenous and exogenous TRIM5α-mediated restriction (35). We thus examined whether TRIM69 isoform B might similarly inhibit the anti-VSIV activity of isoform A. When TRIM69 (isoform A) was constitutively expressed, it conferred potent protection from VSIV-GFP infection (Fig. 3E), and this protection was further enhanced by the presence of inducible myc-tagged TRIM69 (Fig. 3E). In contrast, constitutively expressed TRIM69 isoform B had negligible effect on the ability of isoform A to inhibit VSIV (Fig. 3E), despite being abundantly expressed (Fig. 3F). Thus, although TRIM69 isoform B has no detectable antiviral activity, it does not appear to interfere with the ability of isoform A to block VSIV. It is therefore likely that heteromultimers between isoform A and isoform B either cannot form or are competent to restrict VSIV.

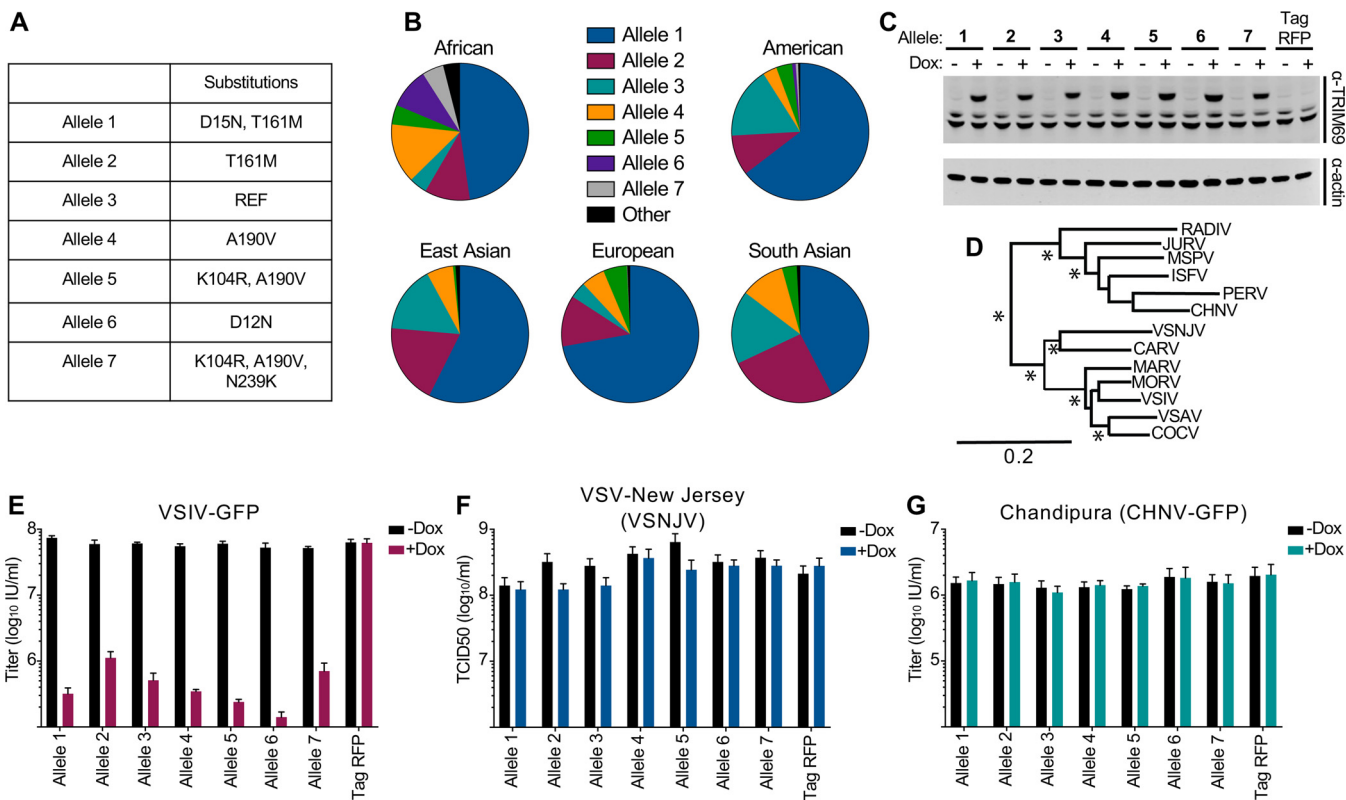


FIG 4 Multiple TRIM69 alleles circulate in human populations. (A) The amino acid substitutions of the most common TRIM69 alleles (as determined via the 1000 Genomes Project). (B) The allelic frequency of the major alleles by geographic region (as determined via the 1000 Genomes Project). (C) MT4 cells were modified to express the seven most common TRIM69 alleles in a doxycycline-inducible fashion. Western blot analysis of myc-TRIM69 expression in cells was performed with and without 24 h of doxycycline treatment. (D) The redrawn phylogeny of common vesiculoviruses (80) is shown (asterisks represent bootstrap proportions higher than 85%). (E to G) The cells described in the legend of panel C were used to examine the ability of divergent TRIM69 alleles to inhibit VSIV-GFP (E), VSNJV (F), and CHNV-GFP (G). Virus titrations were carried out on at least two occasions, and typical results are shown. Mean titers and standard deviations are plotted based on at least three doses (in the linear range).

Multiple TRIM69 alleles circulate in human populations, and TRIM69 exhibits strong signatures of positive selection.

We next analyzed structural variation at the TRIM69 locus in human populations, using data from the 1000 Genomes Project collated by ENSEMBL (36). Interestingly, multiple TRIM69 alleles circulate at high frequencies in human populations. Surprisingly, the human TRIM69 variant [NM_182985](#) (NCBI Reference Sequence) is only the third most common human TRIM69 allele, present at frequencies of ~4% (European) to ~17% (South Asian) in human populations. In light of this, we examined the ability of all the major TRIM69 alleles (with a frequency >5% in at least one population) to inhibit a small panel of vesiculoviruses (Fig. 4). We cloned the seven main alleles into our doxycycline-inducible expression system (Fig. 4A to C) and challenged these cells with a small panel of vesiculoviruses (Fig. 4D to G). In spite of the amino acid variation (Fig. 4A), all seven major alleles conferred potent protection from VSIV infection (Fig. 4E). Although some variation in the magnitude of protection was observed, we attributed this to slight variations in TRIM69 expression levels, as opposed to variation in the anti-VSIV activities of the different alleles (Fig. 4C). Upon further viral challenges, TRIM69 again exhibited exquisite antiviral specificity as none of the TRIM69 human alleles inhibited either VSV New Jersey (VSNJV) (Fig. 4F) or Chandipura virus (37) (CHNV-GFP) (Fig. 4G), both of which are closely related to VSIV (Fig. 4D).

Since multiple TRIM69 alleles currently circulate in human populations and because antiviral TRIM proteins can possess strong signatures of positive selection (38), we conducted positive-selection analysis of TRIM69 sequences from primates. We retrieved and aligned the TRIM69 coding region from 18 primate species representing >40

million years of divergent evolutionary pressures (39). Using the maximum likelihood approach in PAML (40), we tested whether models that permit positive selection on individual codons (ratio of nonsynonymous to synonymous changes [dN/dS] of >1) were a better fit to these data than models that do not allow positive selection. In each case, permitting sites to evolve under positive selection gave a better fit (Fig. 5A and B), with a high proportion of codons exhibiting dN/dS values greater than 1 (32.8% with an average dN/dS of 1.9). These analyses identified six residues exhibiting relatively strong signatures of positive selection (Fig. 5A and B). One of the sites identified using this approach (S404) is within the SPRY domain (the domain that forms the host-pathogen interface that defines the antiretroviral specificity of TRIM5 [38]). These analyses suggest that while the majority of sites (67.2%) in TRIM69 have evolved under purifying selection (in order to maintain the overall structure and function of TRIM69), positive selection has likely occurred at specific sites, perhaps influencing the antiviral activity of TRIM69 (38).

Based on the signatures of positive selection at the TRIM69 locus in primates, we hypothesized that divergent TRIM69 proteins might exhibit divergent antiviral specificities. We therefore cloned a variety of TRIM69 orthologs from a selection of species (including primates and a variety of other mammals) into our doxycycline-inducible expression system. Similar to human TRIM69, orthologs from rhesus macaques, rats, cows, alpacas, dogs, ferrets, and horses all potently inhibited VSIV infection (Fig. 5C). Although the magnitude of inhibition was variable, we attributed the majority of this variability to different TRIM69 expression levels (Fig. 5C). Strikingly, murine TRIM69 did not inhibit VSIV, despite being expressed at higher levels than multiple inhibitory orthologs (Fig. 5C). Furthermore, the anti-VSIV activity of TRIM69 appears to have been lost in the *Mus* genus, as TRIM69 orthologs from *Mus caroli* and *Mus pahari* were also noninhibitory, whereas rat TRIM69 potently inhibited VSIV (Fig. 5D). This is not simply due to the murine orthologs lacking specific cofactors/interactions within human cells, as stable expression of murine TRIM69 (*Mus musculus*) in mouse cells indicated that murine TRIM69 still possessed no apparent anti-VSIV activity (Fig. 5E). Crucially, murine TRIM69 was abundantly expressed in these cells, and human TRIM69 conferred potent protection from VSIV infection when expressed at similar levels in the identical murine background (Fig. 5E and F). Thus, while murine cells support TRIM69-mediated anti-VSIV activity, all tested murine orthologs of TRIM69 have lost the ability to inhibit VSIV.

We also challenged the species variants of TRIM69 with related vesiculoviruses (VSNJV and CHNV), but none of the orthologs considered possessed substantial antiviral activity against these viruses (Fig. 5G and H).

In light of the positive-selection analysis and species-dependent activity of TRIM69, we compared the murine TRIM69 amino acid sequence to sequences of the restrictive human and rat TRIM69 variants (Fig. 6). While human and mouse TRIM69 sequences were relatively well conserved (79% identity), the rat and mouse variants (which were the closest orthologs we tested that displayed differential activity against VSIV), appeared highly similar, differing at only 38 amino acid positions (92% identity). Although site-specific signatures of positive selection were detected in TRIM69, all of the signature sites were conserved between rats and mice (Fig. 6). Thus, the genetic basis of the differential anti-VSIV activity observed in rodent TRIM69 variants is currently unknown.

The VSIV phosphoprotein confers sensitivity/resistance to TRIM69. The short generation times inherent to the lifecycles of most viruses mean that resistance to inhibition can be rapidly selected *in vitro* (5, 27, 41, 42). Approaches using *in vitro* evolution can rapidly identify antiviral sensitivity/resistance determinants in viruses targeted by antiviral factors (41, 43). We used a diverse swarm of replication-competent, full-length (FL) VSIV-GFP (44) that had been propagated in mammalian cells. This parental virus stock was potently inhibited by TRIM69 following overnight infection (Fig. 7A). We used this virus to inoculate a culture expressing TRIM69, using a dose in which $<1\%$ of cells were GFP positive following overnight incubation. Four days later, VSIV had begun to overwhelm this culture, and the supernatant was filtered and

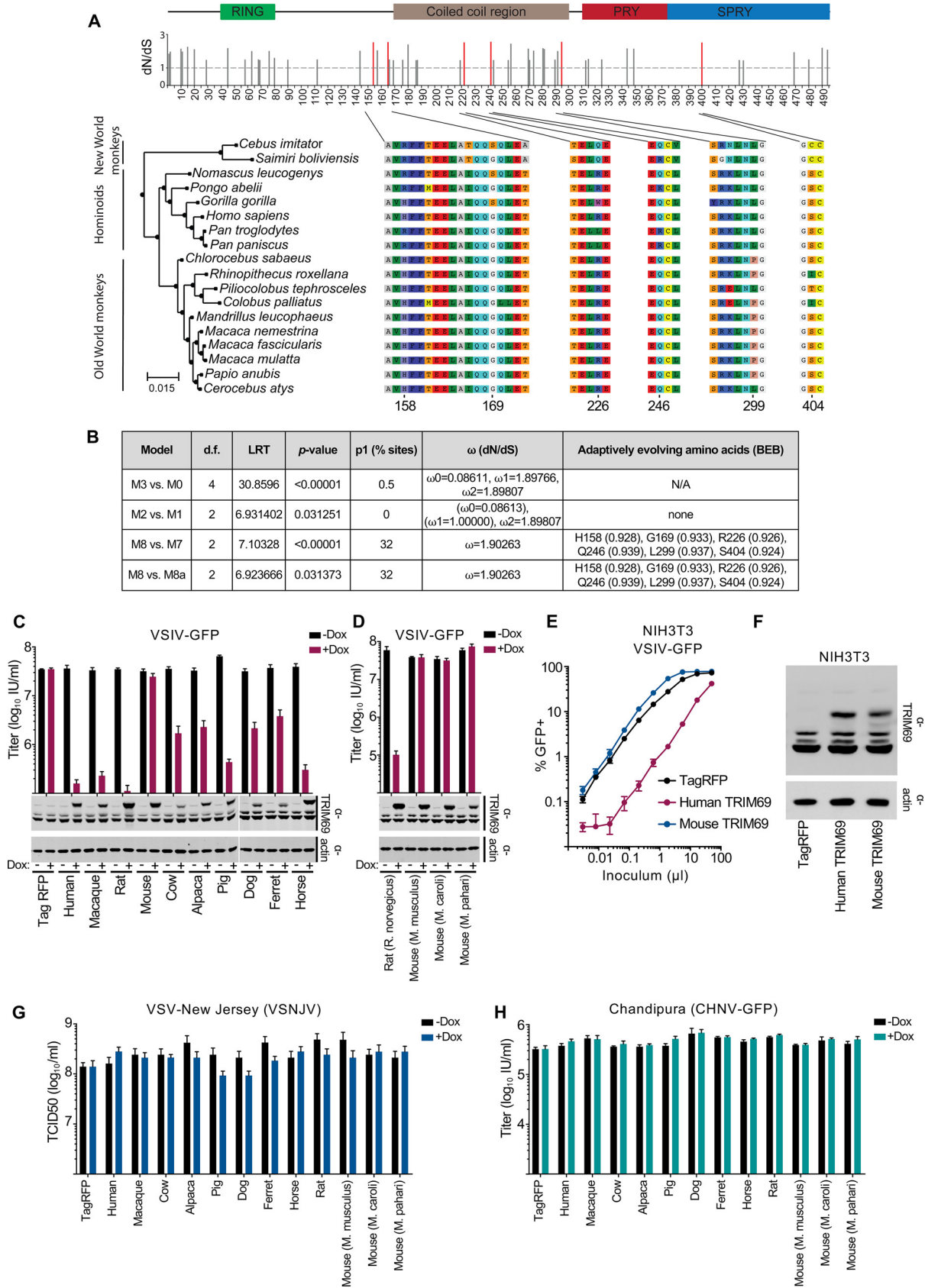


FIG 5 TRIM69 exhibits signatures of positive selection, and anti-VSIV activity has been lost in the *Mus* lineage. (A) The diagram at top illustrates the conserved domains of TRIM69 based on the Conserved Domains Database (CDD), version 3.16, from NCBI. The bar chart at bottom (Continued on next page)



FIG 6 Amino acid alignment of human, rat, and mouse TRIM69 proteins. An amino acid alignment of TRIM69 proteins from human (*Homo sapiens*, GenBank accession no. [NM_182985](#)), rat (*Rattus norvegicus*, [NM_001013160](#)), and mouse (*Mus musculus*, [NM_080510](#)), aligned using ClustalW, is shown. Protein domains are highlighted (based on Conserved Domains Database [CDD], version 3.16, from NCBI), and positions where the murine variant differs from human and rat are highlighted in bold type. Sites identified as positively selected in primates are highlighted with a star (★). The arrow denotes the start of isoform B (preceded by amino acids one and two [ME] from the first coding exon).

transferred to a new culture (also induced to express TRIM69). In this second passage, VSIV replicated far more efficiently in the presence of TRIM69, suggesting that resistance had emerged. Such rapid acquisition of resistance is a documented property of VSIV populations, and VSIV fitness has been previously shown to increase >1,000-fold in a single passage (within a new cellular environment) (45). We titrated the filtered supernatant containing the TRIM69-passaged swarm, in the presence and absence of TRIM69, and observed that VSIV had been selected to resist TRIM69 inhibition (Fig. 7A). We sequenced the viral population and observed four substitutions that had been selected to near uniformity in the viral swarm (Fig. 7B and C). These substitutions included two synonymous changes and two nonsynonymous substitutions. Because we had previously observed that the VSV-G protein was not targeted by TRIM69 when used to pseudotype HIV-1 (Fig. 1E), we reasoned that one substitution, E92K in VSIV-G, was unlikely to confer resistance to TRIM69. This left only one nonsynonymous substitution, D70Y, located in the VSIV phosphoprotein (P protein) that might confer TRIM69 resistance. We mutated this residue in isolation in the FL VSIV-GFP plasmid background and rescued the parental and D70Y mutant viruses. While the rescued parental virus was potently inhibited by TRIM69, the P protein D70Y mutant was completely insensitive to inhibition by TRIM69 (Fig. 7D). Thus, the VSIV P protein is the genetic target of TRIM69 and can determine sensitivity or resistance to TRIM69. Moreover, just a single amino acid within the P protein can determine TRIM69 sensitivity. We next considered the variation at position 70 in VSIV sequences deposited in GenBank. Interestingly, VSIV was uniformly aspartic acid at position 70 (Fig. 7E), suggesting that the D70Y escape mutant either cannot thrive *in vivo* or that TRIM69 does not exert enough pressure to provide a selective advantage to this variant (within these sequences). Importantly,

FIG 5 Legend (Continued)

represents the *dN/dS* values of the sites with positive selection. The six sites with statistically significant positive selection (PAML M8 with Bayes Empirical Bayes [BEB], *P* > 0.9) are shown in red. The phylogenetic relationship between the 18 sequences spanning the hominoids is shown on the left, with the regions of the alignment with statistically significant positive sites shown numbered on the right. (B) The results of the chi-square test comparing the PAML models is shown in the table along with the proportion of sites under positive selection and the average *dN/dS* for those sites. (C) MT4 cells were modified to express myc-TRIM69 orthologs from multiple species in a doxycycline-inducible fashion. Western blot analysis of TRIM69 expression in cells with and without 24 h of doxycycline treatment is shown beneath the titers of VSIV-GFP (16 h postinfection) in the presence and absence of doxycycline treatment. (D) The experiment as described for panel C, examining TRIM69 from rat and divergent mice. (E) NIH 3T3 cells were modified to stably express TagRFP or human or mouse TRIM69 (LHCX) before being infected with serially diluted VSIV-GFP. (F) Western blot analysis of TRIM69 expression in the cells from the experiment described by panel E. (G to H) The cells from the experiment described in panel C were used to determine the titers of VSNJV (G) and CHNV-GFP (H). In all cases, virus titrations were carried out on at least two occasions, and typical results are shown. Mean and standard deviations are plotted, and titers are based on at least three doses (in the linear range). LRT, likelihood ratio test.

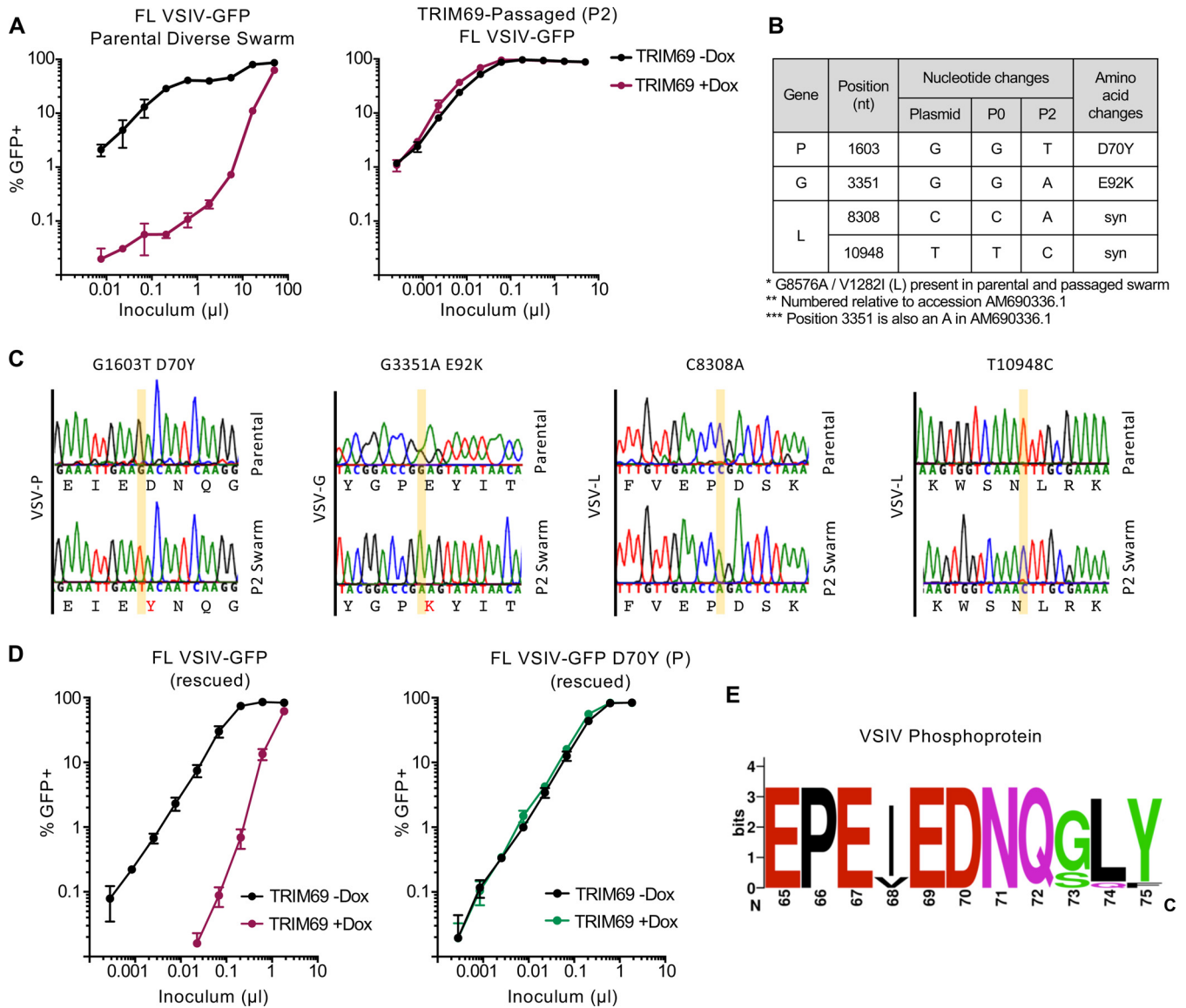


FIG 7 The VSIV phosphoprotein is a genetic susceptibility/resistance determinant of TRIM69 anti-VSIV activity. (A) Serially diluted infection of MT4 cells modified to express doxycycline-inducible human TRIM69 with either parental FL-VSIV-GFP or FL-VSIV-GFP passaged twice (P2) in the presence of human TRIM69 is shown. (B) The passaged and parental swarms were sequenced, and the listed changes were selected to near uniformity in the passed population. (C) Sequencing chromatograms of directly sequenced PCR products amplified from the reverse-transcribed viral swarms are shown. (D) Titrated infection of the cells described for panel A with the parental virus and the D70Y (P) mutant FL-VSIV-GFP, rescued in parallel. In all cases, virus titrations were carried out on at least two occasions, and typical results are shown. Mean and standard deviation are plotted. (E) A WebLogo (weblogo.berkeley.org) sequence logo of the region of the phosphoprotein containing D70 from an alignment of 14 nonredundant protein sequences of VSIV compiled from 50 sequences retrieved from GenBank.

antiviral factors that target highly conserved viral peptides are more likely to form an effective antiviral defense.

TRIM69 inhibits VSIV but not DENV-2. During the preparation of the manuscript, it was reported that TRIM69 is an ISG that targets dengue virus type 2 (DENV-2) through an interaction with NS3 that targets NS3 for degradation (33). This TRIM69-mediated degradation of NS3 interrupts the life cycle of DENV-2 (33). This observation was of immediate interest to us as it is unusual for an antiviral factor to specifically target viruses as divergent as DENV-2 (a positive-sense ssRNA virus) and VSIV (a negative-sense ssRNA virus). Moreover, murine TRIM69, which is inactive against VSIV, was reported to inhibit DENV-2 (33), suggesting that species variants of TRIM69 might have divergent antiviral specificities. We thus compared the ability of TRIM69 to inhibit

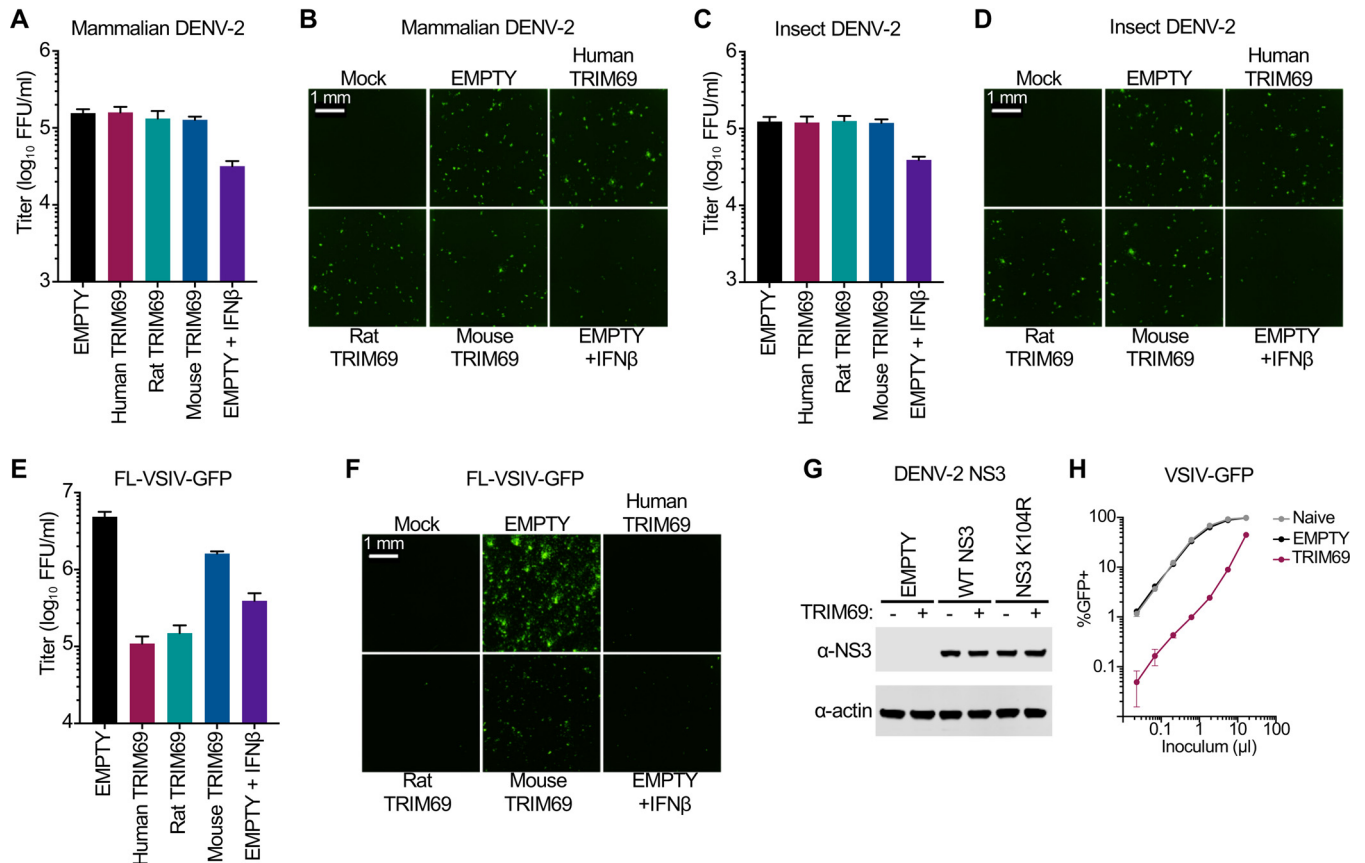


FIG 8 TRIM69-mediated inhibition of DENV-2 was not detected under conditions that restrict VSIV. Vero cells were modified to stably express human, rat, and mouse TRIM69 or were transduced with the corresponding empty vector (SCRPSY). Where indicated, cells transduced with the empty vector were also pretreated with 1,000 units of IFN- β . Cells were then challenged with DENV-2 propagated in Vero cells (mammalian DENV-2) (A and B) or with DENV-2 produced from *Aedes albopictus* C6/36 cells (insect DENV-2) (C and D). At 48 h after infection, cells were fixed and stained for DENV-2 infection, and infected foci were imaged (representative images are shown panels B and D) and enumerated (A and C) using a Celigo imaging cytometer. (E and F) As described in the legend for panels A to D, Vero cells were infected with FL-VSIV-GFP, fixed, and analyzed 16 h after infection. (G) HEK 293T cells were modified to stably express human TRIM69 or were transduced with the corresponding empty vector (SCRPSY). Empty (-) and TRIM69-expressing (+) cells were transfected with DENV-2 NS3, DENV-2 NS3 K104R, or empty expression plasmids, and NS3 expression was analyzed 48 h later using Western blotting. (H) In parallel with the experiment shown in panel G, functional TRIM69 expression in equivalent HEK 293T cells was assessed by titrated infection with VSIV-GFP. In all cases, virus titrations were carried out on at least two occasions, and typical results are shown. Means and standard deviations are plotted.

DENV-2 and VSIV in the same experiment. Because Vero cells are susceptible and permissive to both DENV-2 and VSIV, we selected these cells as the background for our experiments and generated Vero cells that stably expressed human, rat, or mouse TRIM69 and infected these cells with a titrated challenge of DENV-2 or VSIV-GFP. We used the New Guinea C strain of DENV-2 as this strain was previously reported to be inhibited by TRIM69 (33). Unexpectedly, DENV-2 produced in either mammalian or insect cells was not inhibited by TRIM69 under these conditions (Fig. 8A to D). In contrast, VSIV was potently inhibited by human and rat, but not mouse, TRIM69 in parallel experiments (Fig. 8E and F).

Because the previously published work had not specifically investigated exogenous TRIM69 expression in Vero cells, we examined whether TRIM69 expression in HEK 293T cells would induce the degradation of transfected NS3 but not NS3 K104R (in order to recapitulate the published observations) (33). Surprisingly, TRIM69 had no effect on NS3 expression levels (Fig. 8G). In contrast, VSIV was potently blocked in parallel experiments using the equivalent cells (Fig. 8H). We conclude that DENV-2 is not always inhibited by TRIM69, even under conditions where TRIM69 exhibits substantial antiviral activity against VSIV.

The anti-VSIV activity of TRIM69 is not dependent upon IFN signaling or E3 Ub ligase activity. TRIM69 has a RING domain that is predicted to have E3 ubiquitin (Ub)

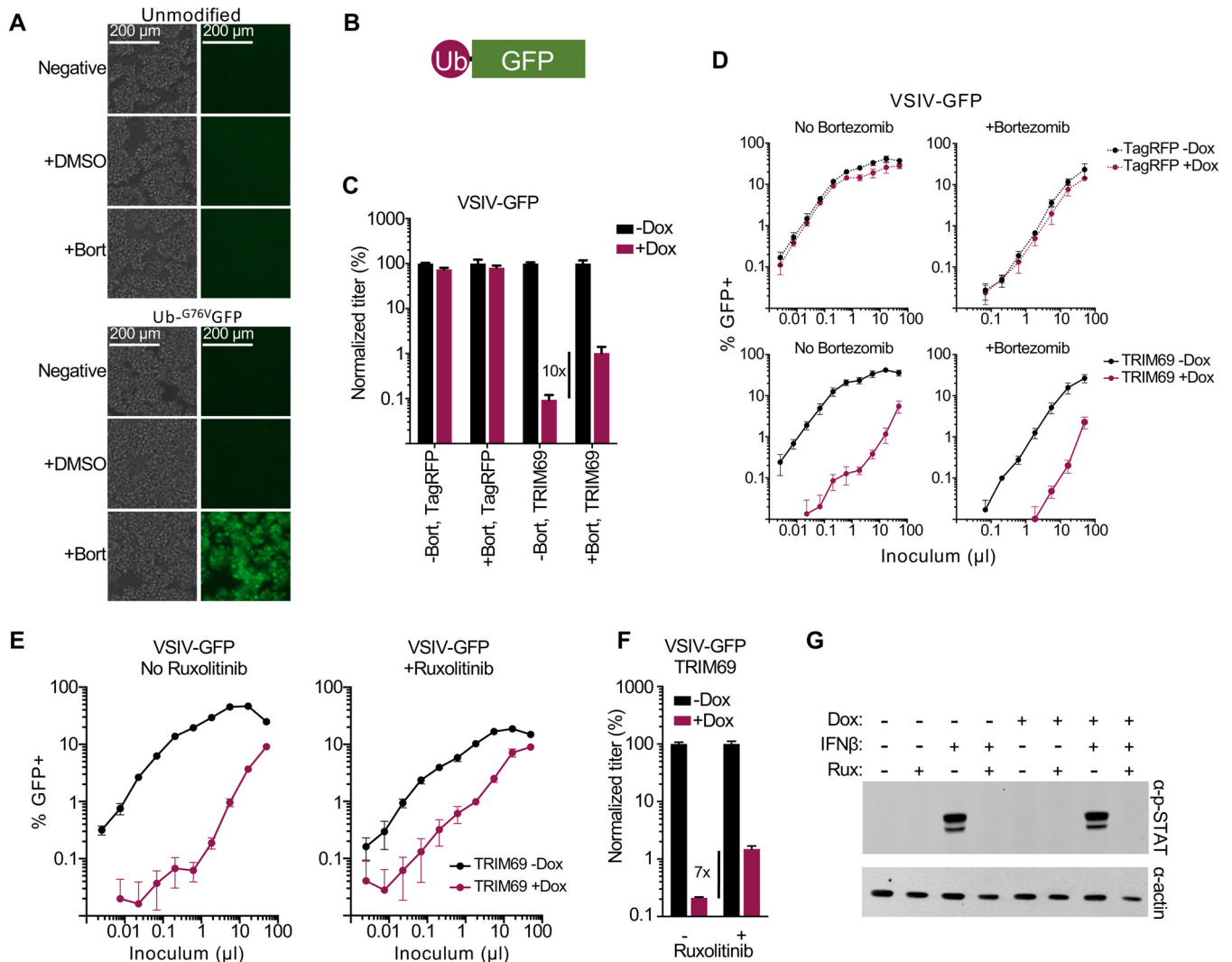


FIG 9 TRIM69-mediated antiviral activity does not require the proteasome or IFN signaling. (A) Phase-contrast and epifluorescence images (EVOS FL microscope) of unmodified MT4 cells or MT4 cells modified to express Ub-G76V-GFP in the presence or absence of 50 nM bortezomib (proteasome inhibitor). (B) An illustration of Ub-G76V-GFP. (C and D) MT4 cells modified to express inducible Myc-TagRFP or myc-TRIM69 (human) were treated or not treated with doxycycline (24 h) before being infected with VSIV-GFP (16 h) in the presence or absence of 50 nM bortezomib. Normalized titers are shown in panel C of the titration curves shown in panel D. (E and F) The same experiment as described for panels C and D, but examining VSIV-GFP in the presence of inducible myc-TRIM69 with or without 2 μM ruxolitinib (JAK1/2 inhibitor). Normalized titers are shown in panel F of the titration curves shown in panel E. (G) Phospho-STAT1 expression in the presence and absence of 2 μM ruxolitinib incubated for 24 h in the presence or absence of 1,000 units of IFN-β was examined in MT4 cells (in the presence or absence of doxycycline-inducible myc-TRIM69) and measured in parallel with the cells used in the experiment shown in panel E. In all cases, virus titrations were carried out on at least two occasions, and typical results are shown. Means and standard deviations are plotted.

ligase activity. Moreover, proteasomal degradation has previously been reported to be involved in the TRIM69-mediated inhibition of DENV-2 (33). In addition, TRIM69 isoform B (which lacks a RING domain) possesses no anti-VSIV activity (Fig. 3C). We therefore considered whether inhibiting proteasomal degradation might affect TRIM69 antiviral activity. As a less toxic alternative to the proteasome inhibitor MG132, we used bortezomib (Bort), an inhibitor of the 26S proteasome, which is also licensed for clinical use (46, 47). In order to validate the efficacy of inhibition, we transduced cells with a lentiviral vector encoding ubiquitin fused to GFP. This fusion protein is rapidly degraded, and GFP expression is not visible under normal culture conditions (Fig. 9A and B). However, when the 26S proteasome was inhibited by bortezomib treatment, abundant GFP expression was visible, suggesting that proteasomal inhibition was efficient in our culture system. In parallel experiments, we considered the ability of proteasome inhibition to influence TRIM69-mediated restriction of VSIV. When normal-

ized to infection in the absence of TRIM69, proteasomal inhibition appeared to partially rescue the restriction of VSIV (Fig. 9C). However, bortezomib treatment caused noticeable toxicity in these experiments, consistent with bortezomib's proapoptotic and anti-tumor cell growth properties (47). Visual inspection of the titration curves indicated that the majority of the rescue was due to reduced VSIV infection in control cells (in the presence of bortezomib), as opposed to proteasomal inhibition actually enhancing infection in the presence of TRIM69 (Fig. 9D). Importantly, TRIM69 potently restricted VSIV (>50-fold) in the presence of efficient proteasome inhibition, indicating that proteasomal degradation is not necessary for effective TRIM69-mediated restriction.

Many TRIM proteins are involved in antiviral signaling and appear to have antiviral activity because their exogenous expression promotes or potentiates a polygenic antiviral state (30, 31). Although the observation that most viruses escape inhibition by TRIM69 suggests that a polygenic response is not involved, we investigated whether TRIM69 could inhibit VSIV in the absence of JAK-STAT signaling. We therefore used the Janus kinase (JAK) inhibitor ruxolitinib to block interferon signaling in TRIM69-expressing cells (48). We then examined the ability of TRIM69 to block VSIV infection in the absence of IFN signaling. As with bortezomib, some toxicity was observed, and ruxolitinib slightly reduced the level of infection in the absence of TRIM69 (Fig. 9E and F). Thus, the majority of the apparent ~7-fold rescue (Fig. 9F) was caused by reduced infection in the absence of TRIM69 (as opposed to ruxolitinib solely enhancing infection in the presence of TRIM69). However, in contrast to bortezomib, ruxolitinib did modestly increase the amount of VSIV infection in the presence of TRIM69 (increasing the titer ~2.5-fold) (Fig. 9E). Importantly, the ruxolitinib treatment effectively blocked IFN signaling, and no phosphorylated STAT1 was detectable following IFN treatment in the presence of ruxolitinib (Fig. 9G). Notably, TRIM69 expression alone was insufficient to trigger the phosphorylation of STAT1 (Fig. 9G), and TRIM69 potently blocked VSIV (>20-fold) in the presence of ruxolitinib. Thus, IFN signaling is not necessary for TRIM69 to inhibit VSIV (although JAK-STAT signaling might modestly enhance this inhibition).

DISCUSSION

Although vesiculoviruses can be particularly sensitive to IFN-induced inhibition, the specific ISGs that mediate the anti-VSIV activity of IFNs (and how this inhibition is achieved) have not yet been fully defined. Here, we show that one ISG, TRIM69, can potently and specifically inhibit VSIV. Moreover, the high degree of specificity of this inhibition overwhelmingly suggests that this inhibition is direct. TRIM69 potently blocked VSIV, whereas other vesiculoviruses (and more divergent RNA viruses) were entirely resistant. Furthermore, the inhibition of VSIV appeared to be remarkably specific as a single substitution conferred complete resistance to TRIM69. Thus, although we cannot exclude the possibility that TRIM69 expression elicits some kind of antiviral signaling, such a signaling event would have to be independent of proteasomal degradation and JAK-STAT signaling and also result in an outcome that specifically targeted VSIV. Therefore, the more parsimonious explanation is that TRIM69, or a complex containing TRIM69, directly targets VSIV (and interferes with the virus life cycle). This potentially adds TRIM69 to an expanding list of directly antiviral TRIM proteins that includes the classical restriction factors TRIM5 (35) and PML (49). Nonetheless, inhibition of IFN signaling modestly rescued VSIV infection, and TRIM69 KO slightly reduced the IFN-induced inhibition of HIV-1. Thus, it is possible that TRIM69 might also play a signaling role analogous to the signaling capacity of established directly antiviral factors such as TRIM5, TRIM21, and tetherin (50–52).

Perhaps the most surprising aspect of the highly specific anti-VSIV activity of TRIM69 was that DENV-2, previously reported to be inhibited by TRIM69 (33), was not inhibited in our experiments. Importantly, this lack of TRIM69 sensitivity was observed while parallel cultures (of the equivalent cells) fiercely resisted VSIV infection. There are many possible explanations for these apparently contradictory observations. The most likely explanation is that due to the highly specific nature of TRIM69-mediated inhibition, some aspect of the virus strain, cellular background, or method used led to DENV-2

appearing insensitive to inhibition (in our experiments). We were careful to use the same strain as used previously (specifically, the New Guinea C strain, which we obtained from Public Health England). We confirmed the presence of the TRIM69-sensitive lysine (at position 104 of NS3) in our virus stocks, and more work will be required to understand why we did not observe DENV-2 inhibition in the face of antiviral TRIM69. Importantly, with both VSIV and DENV-2, a single amino acid substitution conferred resistance to TRIM69. Moreover, we considered only a single human allele (allele 3), which differs at two residues from the variant used previously (GenBank accession no. [AY305385.1](#)) (33, 53). Thus, seemingly minor differences in viral strains could easily reconcile these apparently contradictory observations.

Although we do not know how TRIM69 impedes VSIV, the block must occur relatively early in the viral life cycle. TRIM69 is able to block VSIV prior to the expression of GFP, which in the case of the rVSVΔG-GFP system is encoded in place of the VSV-G protein. Thus, the TRIM69-mediated block must occur at a step prior to translation of VSV-G subgenomic RNA (sgRNA). In the absence of direct evidence, the D70Y mutation in the VSIV phosphoprotein does provide some potential mechanistic clues. Importantly, D70 is present in a region of VSV-P that is heavily phosphorylated (phosphorylation of residues 60, 62, and 64 has been described previously) (54). Phosphorylation of these sites has been proposed to be important in P protein dimerization and interaction with the L protein (large polymerase protein) (55–59), and phosphorylation of this region is essential for functional RNA-dependent RNA polymerase activity (60). Because tyrosine residues are known to be phosphorylated in the VSV-P protein (61), it is therefore tempting to speculate that a tyrosine at position 70 could be phosphorylated and that this phosphorylation somehow overcomes the block mediated by TRIM69. A speculative mechanism that involves TRIM69-mediated inhibition of VSIV RNA-dependent RNA polymerase activity (by inhibiting the association of P and L proteins), preventing subgenomic RNA transcription, would be entirely consistent with the early block described herein.

Although TRIM69 isoform B (which lacks the RING domain) does not possess anti-VSIV activity, proteasomal inhibition was unable to rescue VSIV infectivity. Thus, it is unclear whether functional E3 ubiquitin ligase activity is required to inhibit VSIV. Importantly, isoform B is ~30% shorter than isoform A, and it is possible that such a large deletion perturbs the tertiary or quaternary structure of TRIM69. Such an inability to form multimers could simultaneously explain why isoform B is both inactive and lacks dominant negative activity. More work will be required to understand the role that E3 ubiquitin ligase activity plays in TRIM69's immune role.

The N-terminal regions of vesiculoviral P proteins are relatively divergent, providing a possible explanation for the observed insensitivity of VSNJV and CHNV to TRIM69. Thus, examining the more closely related Morreton virus (MORV), vesicular stomatitis Alagoas virus (VSAV), Cocal virus (COCV), or Maraba virus (MARV) might identify more viruses which are sensitive to TRIM69 and potentially identify further evidence of species specificity. Notably, after analyzing 50 VSIV sequences (deposited in GenBank), we did not observe a tyrosine at position 70 of VSIV-P in any VSIV sequences. This suggests that if TRIM69 substantially inhibits VSIV *in vivo*, the D70Y mutation must be deleterious for some other reason and is therefore negatively selected (despite conferring resistance to TRIM69). Potential explanations include a reduction in replicative fitness or sensitization to other immune processes. Although we have not directly compared the replicative fitness of the D70Y mutant to that of the parental virus, virus preps of this mutant have slightly lower titers (less than a 5-fold reduction [our unpublished observations]), providing a possible explanation as to why this mutant was not observed in reported VSIV sequences.

Our failure to identify any viruses other than VSIV that were inhibited by TRIM69 limited our ability to identify whether species variants of TRIM69 possess divergent antiviral specificities. Despite this, differential activity was observed as anti-VSIV activity has apparently been lost in the *Mus* genus. Whether murine TRIM69s have been

selected to target other viruses or whether murine orthologs have no antiviral activity at all remains to be determined.

The lack of anti-VSIV activity conferred by murine TRIM69 could have important implications for our understanding of how the IFN response constrains VSIV. Many key VSIV experiments have been conducted in mice (15, 16), and it will be important to establish in the future whether nonmurine variants of TRIM69 possess anti-VSIV activity *in vivo*, potentially limiting the ability of VSIV to invade and colonize certain tissues. It is possible that the potent inhibition of VSIV observed *in vitro* will be recapitulated *in vivo*. In this way, IFN-induced TRIM69 might inhibit natural VSIV infections and similarly influence the safety and/or efficacy of therapeutic interventions (based upon VSIV). Thus, an improved understanding of how TRIM69 inhibits VSIV may help us to better understand VSIV pathogenesis and eventually lead to tangible benefits in the clinical use of VSIV derivatives.

MATERIALS AND METHODS

Cells and viruses. Adherent HEK 293T, BHK-21, BSRT7/5 cells (modified to stably express T7 RNA polymerase [62]), NIH 3T3, and Vero cells were propagated from lab stocks maintained in Dulbecco's modified Eagle's medium (DMEM) supplemented with 9% fetal calf serum (FCS) and 10 $\mu\text{g}/\text{ml}$ gentamicin. CADO-ES1 semiaherent cells were purchased from the DSMZ (ACC 255), and suspension MT4 cells were expanded from lab stocks and maintained in RPMI medium supplemented with 9% FCS and 10 $\mu\text{g}/\text{ml}$ gentamicin. C6/36 cells (*Aedes albopictus*) were propagated from existing lab stocks and maintained in L-15 (Leibovitz) medium with GlutaMAX, 10% fetal bovine serum, 10% tryptose phosphate broth, and 1% penicillin-streptomycin (pen/strep). Transduced cells were selected and cultured in medium additionally supplemented with 2 $\mu\text{g}/\text{ml}$ puromycin (Melford Laboratories) or 200 $\mu\text{g}/\text{ml}$ of hygromycin B (Invitrogen).

The VSIV-GFP virus (rVSV Δ G-GFP) competent to undergo a single round of infection but not encoding the VSV-G envelope (rVSV- Δ G-GFP decorated with VSV-G expressed in *trans*) system was used (28). Virus stocks were generated as described previously (42). Briefly, HEK 293T cells were transfected with a VSV-G expression plasmid. The next day, the cells were infected with rVSV- Δ G-GFP at a multiplicity of infection (MOI) of 1. Progeny virus-like particle (VLP) stocks were harvested at 24 h postinfection and clarified using a 0.45- μm -pore-size filter. The replication-competent FL-VSIV-GFP, VSIV, and VSNJV viruses were a generous gift from Megan Stanifer (Heidelberg University). Virus stocks were generated through infection of BHK-21 cells using a low MOI. Once cytopathic effect (CPE) was readily apparent, supernatants were harvested and clarified using a 0.45- μm -pore-size filter.

The D70Y mutant (VSV-P) was made using an Agilent QuikChange Lightning site-directed mutagenesis kit, in accordance with the manufacturer's instructions, using the parental FL-rVSV-GFP plasmid as the template [pVSV1(+)-GFP] (44) and the following oligonucleotides, 5'-GCT TCC GGA TCT GGT ACA TAC AAG CCT TGA TTG TAT TCA ATT TCT TCA GAT TCT GT-3' and 5'-TGA TTC TGA CAC AGA ATC TGA ACC AGA AAT TGA ATA CAA TCA AGG CTT GTA TGT ACC AG-3'. The entire coding region was subsequently sequence verified to confirm the presence of the sole D70Y (VSV-P) mutation. To rescue the parental and mutant virus, BSR-T7 cells were seeded and infected with fowlpox T7 virus (equivalent to an MOI of \sim 2 determined using DF-1 cells) (63). After 1 h of incubation, 1.66 μg of the FL-VSIV-GFP rescue plasmid [pVSV1(+)-GFP] or mutant D70Y [pVSV1(+)-GFP P-D70Y] was cotransfected with pBS-N (0.83 μg), pBS-P (0.5 μg), and pBS-L (0.33 μg) (KeraFAST) using FuGENE6 (Promega). After 48 h, GFP-positive cells and CPE were observed in the transfected BSR-T7 cells. Supernatant containing VSIV was harvested and clarified using a 0.45- μm -pore-size filter and stored at -80°C . VSIV was propagated in BHK-21 cells in T-25 flasks. Cells were infected at a low MOI of VSV harvested from BSR-T7 cells. At 48 h postinfection (or when the majority of cells were GFP positive), supernatant was harvested and clarified using a 0.45- μm -pore-size filter.

DENV-2 was obtained from Public Health England (catalogue number 0006041v). The NS3 of the DENV-2 stocks (propagated in Vero cells) used herein was directly sequenced. Briefly, RNA was extracted from infected cells using the same approaches described below for passaged FL-VSIV-GFP, and the NS3 region was amplified using the primers 5'-CGA AGA GGA AGA ACA AAT ACT GAC C-3' and 5'-GAT TGT ACG CCC TTC CAC CTG CTT C-3'; PCR products were sequenced using these primers and an additional primer (5'-GTG GAG CAT ATG TGA GTG CTA TAG C-3'). The NS3 sequence differed by one amino acid, a threonine at position 442, from GenBank accession number [AAC59275](#) (strain New Guinea C).

The replication-competent HIV-1 proviral clone NHG (GenBank accession no. [JQ585717](#)) and Δenv derivatives have been described previously (5, 64). Virus stocks were generated through transient transfection of HEK 293T cells in isolation (NHG) or in conjunction with a VSV-G expression plasmid (NHG Δenv). The single-cycle HIV-1 lentiviral vector CSGW is a self-inactivating, VSV-G-pseudotyped lentiviral vector that encodes GFP expressed from an internal spleen focus-forming virus (SFFV) long terminal repeat (LTR) (65), packaged using GagPol derived from HIV-1 NL4-3 (pNLGP). The single-round RVFV system has also been described previously (66). Briefly, BHK-Rep cells were transiently transfected with pCAGGs-M. The cells were washed the following day, and supernatant was harvested at 48 h posttransfection and clarified using a 0.45- μm -pore-size filter.

An NS1-enhanced green fluorescent protein (EGFP) construct expressing influenza A/Puerto Rico/8/1934 (H1N1) (PR8) virus was designed based on the previously described Color-Flu system (67). A DNA

sequence was synthesized (Genewiz) with flanking BsmBI sites corresponding to the NS segment of PR8 (GenBank accession no. [EF467817.1](#)) in which the NS1 open reading frame (ORF) had been altered to code for a C-terminally EGFP-tagged NS1 protein with a CSGG linker. This was immediately followed in frame by a CSG linker, the 2A protease of porcine teschovirus (PTV), and the nuclear export protein (NEP) ORF. A splice acceptor site in the NS1 ORF was removed by introducing A527C and A530G (numbering is in accordance with GenBank accession no. [EF467817.1](#)). The sequence was subcloned into the pHW2000 reverse genetics plasmid. The PR8-NS1-EGFP virus was rescued using a well-established reverse genetics system previously described (68), a generous gift from Ron Fouchier.

Retroviral vectors and plasmids. The SCRPSY (GenBank accession no. [KT368137.1](#)) and doxycycline-inducible (LKOΔ-MycTagRFP-IP) lentiviral vectors have been previously described (5, 43). The retroviral vector LHSXN (a gift from T. Zang and P. Bieniasz) is a derivative of LHCX (Clontech) modified to contain the multiple-cloning site (MCS) 5'-AAG CTT GGC CGA GAG GGC CGA AAA CGT TCG CGG CCG CGG CCT CTC TGG CCG TTA AC-3' between the HindIII and HpaI sites (highlighted in italics) of LHCX. All human and species variants of TRIM69 were synthesized by Genewiz, based on NCBI sequences of the longest isoform, unless otherwise noted, from the following (GenBank accession no.): human (human isoform A, [NM_182985.4](#); isoform B, [NM_080745.4](#); isoform C, [NM_001301144.1](#); isoform D, [NM_001301145.1](#); isoform E, [NM_001301146.1](#)), macaque (*Macaca Mulatta*, [XM_015142131.1](#)), rat (*Rattus Norvegicus*, [BC091171](#) [clone IRBPp993F0532D, Image ID 7132390; Source Bioscience]), mouse (*M. musculus*, [BC050815](#) [clone IRAWp5000E114D, Image ID 6774293; Source Bioscience]; *M. caroli*, [XM_021183811.1](#); *M. pahari*, [XM_021193471.1](#)), cow (*Bos indicus*, [XM_019967990.1](#); edited to change an ambiguity base at position 547 to a C to match the sequence of *Bos taurus*, [XM_015473308](#)), alpaca (*Vicugna pacos*, [XM_015237089.1](#); edited to remove 55 amino acids from the start of the sequence and replace with ATGGAG [ME] that is found in all other TRIM69 species variants), pig (*Sus scrofa*, Ensembl no. ENS-SSCT00000005168; edited to remove a 5' K and replace with ATGGAG [ME]), dog (*Canis lupus*, [XM_535459.6](#)), ferret (*Mustela putorius furo*, [XM_004751292.2](#)), and horse (*Equus caballus*, [XM_014733851](#)). Sequences were cloned (using directional SfiI sites) into pSCRPSY, pLKOΔ-Myc-IP, or pLHSXN as indicated in the text, figure, or figure legend. Human allelic variants were cloned using overlap extension PCR and the following oligonucleotides: allele 1, 5'-CTC TCT GGC CGA GAG GGC CAT GGA GGT ATC CAC CAA CCC CTC CAA CAT CGA TCC AGG CAA TGT TGA AAT GAA TGA TTC AAT C-3', 3'-TGA CCC TGT TGG ATG GCA AGC TCC ATG AAG AAA TGG ACA GCA TCA GAG ATT TGC AG-5', 5'-GCA AAT CTC TGA TGC TGT CCA TTT CTT CAT GGA GCT TGC CAT CCA ACA GGG TCA AC-3', and 3'-TCT CTC GGC CAG AGA GGC CTT ACT GTG GAT GTA AGA TGT GCA ATG G-5'; allele 2, 5'-CTC TCT GGC CGA GAG GGC CAT GGA GGT ATC CAC CAA CCC CTC CTC-3', 3'-TGA CCC TGT TGG ATG GCA AGC TCC ATG AAG AAA TGG ACA GCA TCA GAG ATT TGC AG-5', 5'-GCA AAT CTC TGA TGC TGT CCA TTT CTT CAT GGA GCT TGC CAT CCA ACA GGG TCA AC-3', and 3'-TCT CTC GGC CAG AGA GGC CTT ACT GTG GAT GTA AGA TGT GCA ATG G-5'; allele 3, 5'-CTC TCT GGC CGA GAG GGC CAT GGA GGT ATC CAC CAA CCC CTC CTC-3', 3'-TGA CCC TGT TGG ATG GCA AGC TCC ATG AAG AAA TGG ACA GCA TCA GAG ATT TGC AG-5', 5'-GCA AAT CTC TGA TGC TGT CCA TTT CTT CAT GGA GCT TGC CAT CCA ACA GGG TCA AC-3', and 3'-TCT CTC GGC CAG AGA GGC CTT ACT GTG GAT GTA AGA TGT GCA ATG G-5'; allele 4, 5'-CTC TCT GGC CGA GAG GGC CAT GGA GGT ATC CAC CAA CCC CTC CTC-3', 3'-CAG ATG TAG CTT GTT TTC CTT GTG AGC AAC AAT AGC TTC CTT CTG CAT GTT CCT CAG GG-5', 5'-CCT GAG GAA CAT GCA GAA GGA AGC TAT TGT TGC TCA CAA GGA AAA CAA GCT ACA TCT GC-3', and 3'-TCT CTC GGC CAG AGA GGC CTT ACT GTG GAT GTA AGA TGT GCA ATG G-5'; allele 5, 5'-CTC TCT GGC CGA GAG GGC CAT GGA GGT ATC CAC CAA CCC CTC CTC-3', 3'-GTG GAT GGC CCT TGA GTA AGG GAT TCC TAA TCT CTA CCA ACT TGT CCA GTA CAG-5' 5'-GTA CTG GAC AAG TTG GTA GAG AAG ATT AGG AAG TTA CCC TTA CTC AAG GGC CAT CCA CAG-3', and 3'-TCT CTC GGC CAG AGA GGC CTT ACT GTG GAT GTA AGA TGT GCA ATG G-5'; allele 6, 5'-CTC TCT GGC CGA GAG GGC CAT GGA GGT ATC CAC CAA CCC CTC CAA CAT CAA TCC AGG CGA CTA TGT TGA AAT GAA TG-3', and 3'-TCT CTC GGC CAG AGA GGC CTT ACT GTG GAT GTA AGA TGT GCA ATG G-5'; allele 7, 5'-CTC TCT GGC CGA GAG GGC CAT GGA GGT ATC CAC CAA CCC CTC CTC-3', 3'-GAG ACA TTG CTC CTG AAG CTG GCT CAG TTT CAA CTC CAT CTC ATT CAA GGC TTT C-5', 5'-GCC TTG AAT GAG ATG GAG TTG AAA CTG AGC CAG CTT CAG GAG CAA TGT CTC TTA GC-3', and 3'-TCT CTC GGC CAG AGA GGC CTT ACT GTG GAT GTA AGA TGT GCA ATG G-5'. Allele 4 was used as a template for allele 5 PCRs, and allele 5 was used as a template for allele 7. The N-terminal fusion of a mutated uncleavable ubiquitin moiety fused to GFP (Ub-G^{76V}GFP) has been described previously (69). Plasmid DNA containing Ub-G^{76V}GFP[pcDNA3.1(+).Ub-G^{76V}GFP], a gift from A. Fletcher, was digested with BamHI and NotI and inserted into the similarly digested lentiviral vector pCSGWΔNotI (65) (a gift from G. Towers and A. Thrasher).

Gene editing was achieved using a lentiGuide-Puro system (70) in accordance with the protocols of the Zhang lab. The following oligonucleotides were used to make TRIM69 guides: 5'-CAC CGC AAC CCT GTA CTG GAC AAG T-3' and 5'-AAA CAC TTG TCC AGT ACA GGG TTG C-3' (guide 1); 5'-CAC CGA AGA AGT TAC CCT TAC TCA A-3' and 5'-AAA CTT GAG TAA GGG TAA CTT C-3' (guide 2). Diploid CADO-ES1 cells were either transduced with vectors encoding Cas9 and the relevant TRIM69-targeting sgRNAs or transduced in parallel with vectors encoding Cas9 and no sgRNA (no guide). Single-cell clones were generated using limiting dilution, and the KO was confirmed by extracting genomic DNA (DNeasy; Qiagen), followed by PCR amplification of the guide target regions in exon 2 using the following oligonucleotides 5'-CAC TTT CAA AGG AGA GAT TAT GTG C-3' and 5'-GAG CAG TCT GGG CTT TCT AAT CAT C-3'. The PCR products were cloned into pGEM-T-Easy (Promega), and multiple clones were Sanger sequenced.

Viral vectors were produced using transient transfection of HEK 293T cells (5 μg of vector/genome plasmid, 5 μg of the relevant GagPol expression vector, and 1 μg of a VSV-G expression plasmid). Vector-containing supernatants were filtered (using a 0.45-μm-pore-size filter) and used to transduce the relevant cell types.

To make the NS3 expression plasmids, the NS3 coding sequence from the DENV-2 New Guinea C strain (nucleotides 6376 to 6756 of GenBank accession no. [KM204118.1](#)) was synthesized (Genewiz) with

a 5' ATG, flanked by 5' HindIII and 3' XbaI sites, and subcloned into pcDNA 3.1(+). The K104R mutation (AAA →AGA) was introduced using Agilent's QuikChange Lightning Mutagenesis kit and the following primers: 5'-GAC GGC TCT TGG ATT TCT TCC AGG CTC CAA TGC-3' and 5'-GCA TTG GAG CCT GGA AGA AAT CCA AGA GCC GTC-3'.

Arrayed ISG expression screening. The ISG screens were executed as described previously (5, 27). Briefly, MT4 cells were seeded in 96-well plates and transduced with ISG-encoding SCRPSY vectors (one ISG per well). At 48 h posttransduction, cells were infected with VSIV-GFP. Following incubation overnight, cells were fixed and analyzed using flow cytometry.

Western blotting. For preparation of cell lysates, cell pellets were resuspended in SDS sample buffer (12.5% glycerol, 175 mM Tris-HCl [pH 8.5], 2.5% SDS, 70 mM 2-mercaptoethanol, 0.5% bromophenol blue). Proteins were subsequently separated on NuPage 4% to 12% Bis-Tris polyacrylamide gels and transferred onto nitrocellulose membranes. Blots were probed with either anti-actin (JLA20 hybridoma; courtesy of the Developmental Studies Hybridoma Bank, University of Iowa), one of two anti-TRIM69 antibodies (catalog no. ab111943 [Abcam] or PA5-12215 [Thermo Fisher]), anti-DENV-2 NS3 (PA5-32199; Thermo Fisher), anti-phospho-STAT1 (Tyr701) (58D6), or anti-c-myc (9E10 hybridoma; Developmental Studies Hybridoma Bank, University of Iowa). Thereafter, membranes were probed with DyLight-labeled goat secondary antibodies (Thermo) and scanned using a LiCor Odyssey scanner.

Virus infections and titrations. For assays using GFP-encoding viruses, cells were seeded in 96-well plates. Adherent and semiadherent cells were seeded 24 h before challenge or treatment whereas suspension cells were seeded immediately prior to infection or treatment. In experiments using doxycycline-inducible TRIM69 expression, cells were treated with 125 ng/ml of doxycycline hyclate (Sigma) 24 h before infection. Where stated in the figures, figure legends, or text, cells were treated with 2 μ M ruxolitinib (INCB018424) (catalog no. S1378-SEL; Stratech), 50 nM bortezomib (2204; Cell Signaling Technology), or 1,000 units of IFN- β (11420-1; PBL Assay Science) immediately before infection (or in the case of IFN- β , 24 h before infection, except for the experiments in Fig. 8, where a 4-h treatment was used). Cells were then infected with titrated challenges of the indicated virus and incubated overnight (~16 h) or for 48 h (HIV-1 and RVFV) prior to fixation using 4% formaldehyde and enumeration of infected GFP-positive cells using flow cytometry.

For quantification of focus-forming units (FFUs), Vero cells were seeded in 96-well plates. The following day, cells were pretreated with IFN- β (24 h at 1,000 U/ml) prior to infection with FL-VSIVGFP or DENV-2 propagated in Vero cells (mammalian) or C6/36 cells (insect). Cells were infected with titrated DENV-2 in DMEM (2% FCS) for 1 h prior to overlay with DMEM (5% FCS, 0.8% carboxymethylcellulose). Forty-eight hours later, cells were fixed (methanol) and permeabilized (0.1% Triton X-100; Fisher). FFUs were visualized using MAB8705 anti-dengue virus complex antibody clone D3-2H2-9-21 (Millipore) and goat anti-mouse Alexa Fluor 488 (A-11001; Thermo Fisher), as described previously (71). As a control, serially diluted FL-VSIV-GFP was examined in parallel and fixed in 4% formaldehyde following overnight incubation (~16 h). The number of fluorescent foci of immunostained DENV-2- and VSIV-infected cells was enumerated using a Celigo imaging cytometer (Nexcelom Bioscience).

For 50% tissue culture infective dose (TCID₅₀) assays, MT4 cells were seeded in 96-well plates and treated with 125 ng/ml of doxycycline hyclate (Sigma) 24 h prior to infection. The cells were infected with eight replicates of 3-fold serially diluted full-length VSIV or VSIV. At 72 h postinfection (hpi), CPE was analyzed, and the TCID₅₀ was calculated using the Spearman and Kärber algorithm and a modified TCID₅₀ calculator from Marco Binder.

DENV-2 NS3 transfections. HEK 293T cells were transduced with either SCRPSY-empty or SCRPSY-TRIM69 and seeded in six-well plates before transfection with 2 μ g of pcDNA (either empty, wild-type DENV-2 NS3, or DENV-2 NS3 K104R mutant). At 48 h posttransfection, cells were lysed in 500 μ l of SDS sample buffer. In parallel, 293T cells transduced with SCRPSY-empty and SCRPSY-TRIM69 were challenged with serially diluted VSV-GFP to demonstrate TRIM69 activity.

VSIV *in vitro* evolution, RNA extraction, PCR, and sequencing. MT4 cells expressing TRIM69 were seeded and induced with doxycycline hyclate (200 ng/ml) 24 h prior to challenge with FL-VSIV-GFP at a low MOI (<1% infection following 16 h of incubation). The level of infection based on the percentage of GFP-positive cells was monitored daily. Once the culture was overwhelmed, supernatant was filtered (0.45- μ m pore size) and used to infect a second culture. Following passage 2, CPE was observed at 24 h postinfection (in the presence of TRIM69). The supernatant of the passaged virus was filtered (0.45- μ m pore size) and stored. Cell pellets were resuspended in TRIzol (Invitrogen), and viral RNA was isolated from infected cells using a hybrid TRIzol and RNeasy extraction (Qiagen) protocol. Viral cDNA was reverse transcribed (SuperScript III) using random hexamer primers. All VSIV coding regions were PCR amplified, and the PCR products were directly sequenced using Sanger sequencing (Eurofins Genomics).

Sequence collection, alignment, and expression analysis. TRIM69 sequences were obtained from publicly available databases such as ENSEMBL and GenBank using TBLASTN (72). The protein sequences were aligned using MAFFT (73), and a codon alignment was generated based on the protein alignment using PAL2NAL (74). The alignment was screened for recombination in HyPhy (75) using single-breakpoint recombination (SBP) and GARD, a genetic algorithm for recombination detection (76). TRIM69 expression in primary human fibroblasts was meta-analyzed from published data (1), and counts per million (CPM) of TRIM69 expression were extracted as described previously (1). TRIM69 expression levels in human cells were assessed by meta-analyzing existing gene expression data through the EMBL-EBI Expression atlas (<https://www.ebi.ac.uk/gxa/home>), leading to the selection of CADO-ES1 cells for TRIM69 knockout.

To explore the amino acid variation surrounding amino acid D70, 50 sequences from NCBI were aligned, and identical sequences were removed from the alignment to produce a nonredundant set of

protein sequences. A WebLogo sequence logo (77) for the protein region was produced using a web server (<https://weblogo.berkeley.edu/>).

Phylogenetics and positive selection analyses. The best substitution model was selected using Bayesian information criteria (BIC) in jModeltest (78), and the maximum likelihood phylogeny was reconstructed with this model in PhyML with 1,000 bootstrap replicates (79). The primate lineage of the gene tree, which is more extensively sampled for species, was used in CODEML (40) to detect sites under positive selection.

ACKNOWLEDGMENTS

We thank R. Fouchier, T. Zang, P. Bieniasz, G. Towers, Andrew Easton, and A. Fletcher for reagents and Andrew Shaw and Adam Fletcher for their helpful discussions, advice, and assistance.

This study was funded by Medical Research Council (MRC) grants MR/K024752/1 (to S.J.W.), MC_UU_12014/10 (to S.J.W. and M.P.), MR/P022642/1 (to S.J.W. and S.J.R.), and MC_UU_12014/12 (to J.H.) and by Wellcome Trust support grant 201366/Z/16/Z (to S.J.R.).

REFERENCES

- Shaw AE, Hughes J, Gu Q, Behdenna A, Singer JB, Dennis T, Orton RJ, Varela M, Gifford RJ, Wilson SJ, Palmarini M. 2017. Fundamental properties of the mammalian innate immune system revealed by multispecies comparison of type I interferon responses. *PLoS Biol* 15:e2004086. <https://doi.org/10.1371/journal.pbio.2004086>.
- Rusinova I, Forster S, Yu S, Kannan A, Masse M, Cumming H, Chapman R, Hertzog PJ. 2013. Interferome v2.0: an updated database of annotated interferon-regulated genes. *Nucleic Acids Res* 41:D1040–1046. <https://doi.org/10.1093/nar/gks1215>.
- Schoggins JW, Wilson SJ, Panis M, Murphy MY, Jones CT, Bieniasz P, Rice CM. 2011. A diverse range of gene products are effectors of the type I interferon antiviral response. *Nature* 472:481–485. <https://doi.org/10.1038/nature09907>.
- Liu SY, Sanchez DJ, Aliyari R, Lu S, Cheng G. 2012. Systematic identification of type I and type II interferon-induced antiviral factors. *Proc Natl Acad Sci U S A* 109:4239–4244. <https://doi.org/10.1073/pnas.11149811109>.
- Kane M, Zang TM, Rihn SJ, Zhang F, Kueck T, Alim M, Schoggins J, Rice CM, Wilson SJ, Bieniasz PD. 2016. Identification of interferon-stimulated genes with antiretroviral activity. *Cell Host Microbe* 20:392–405. <https://doi.org/10.1016/j.chom.2016.08.005>.
- Schoggins JW, Rice CM. 2011. Interferon-stimulated genes and their antiviral effector functions. *Curr Opin Virol* 1:519–525. <https://doi.org/10.1016/j.coviro.2011.10.008>.
- Letchworth GJ, Rodriguez LL, Del Cbarrera J. 1999. Vesicular stomatitis. *Vet J* 157:239–260. <https://doi.org/10.1053/tvj.1998.0303>.
- Johnson KM, Vogel JE, Peralta PH. 1966. Clinical and serological response to laboratory-acquired human infection by Indiana type vesicular stomatitis virus (VSV). *Am J Trop Med Hyg* 15:244–246. <https://doi.org/10.4269/ajtmh.1966.15.244>.
- Fields BN, Hawkins K. 1967. Human infection with the virus of vesicular stomatitis during an epizootic. *N Engl J Med* 277:989–994. <https://doi.org/10.1056/NEJM196711092771901>.
- Olitsky PK, Sabin AB, Cox HR. 1936. An acquired resistance of growing animals to certain neurotropic viruses in the absence of humoral antibodies or previous exposure to infection. *J Exp Med* 64:723–737. <https://doi.org/10.1084/jem.64.5.723>.
- Rubinstein S, Familletti PC, Pestka S. 1981. Convenient assay for interferons. *J Virol* 37:755–758.
- Espert L, Degols G, Gongora C, Blondel D, Williams BR, Silverman RH, Mechti N. 2003. ISG20, a new interferon-induced RNase specific for single-stranded RNA, defines an alternative antiviral pathway against RNA genomic viruses. *J Biol Chem* 278:16151–16158. <https://doi.org/10.1074/jbc.M209628200>.
- Pavlovic J, Zurcher T, Haller O, Staeheli P. 1990. Resistance to influenza virus and vesicular stomatitis virus conferred by expression of human MxA protein. *J Virol* 64:3370–3375.
- Zurcher T, Pavlovic J, Staeheli P. 1992. Mouse Mx2 protein inhibits vesicular stomatitis virus but not influenza virus. *Virology* 187:796–800. [https://doi.org/10.1016/0042-6822\(92\)90481-4](https://doi.org/10.1016/0042-6822(92)90481-4).
- Fenster V, Wetzel JL, Ramachandran S, Ogino T, Stohman SA, Bergmann CC, Diamond MS, Virgin HW, Sen GC. 2012. Interferon-induced Ifit2/ISG54 protects mice from lethal VSV neuropathogenesis. *PLoS Pathog* 8:e1002712. <https://doi.org/10.1371/journal.ppat.1002712>.
- Muller U, Steinhoff U, Reis LF, Hemmi S, Pavlovic J, Zinkernagel RM, Aguet M. 1994. Functional role of type I and type II interferons in antiviral defense. *Science* 264:1918–1921. <https://doi.org/10.1126/science.8009221>.
- Olitsky PK, Cox HR, Syverton JT. 1934. Comparative studies on the viruses of vesicular stomatitis and equine encephalomyelitis (1). *J Exp Med* 59:159–171. <https://doi.org/10.1084/jem.59.2.159>.
- Frank AH, Appleby A, Seibold HR. 1945. Experimental intracerebral infection of horses, cattle, and sheep with the virus of vesicular stomatitis. *Am J Vet Res* 6:28–38.
- Detje CN, Meyer T, Schmidt H, Kreuz D, Rose JK, Bechmann I, Prinz M, Kalinke U. 2009. Local type I IFN receptor signaling protects against virus spread within the central nervous system. *J Immunol* 182:2297–2304. <https://doi.org/10.4049/jimmunol.0800596>.
- Roberts A, Kretzschmar E, Perkins AS, Forman J, Price R, Buonocore L, Kawaoka Y, Rose JK. 1998. Vaccination with a recombinant vesicular stomatitis virus expressing an influenza virus hemagglutinin provides complete protection from influenza virus challenge. *J Virol* 72:4704–4711.
- Mire CE, Matassov D, Geisbert JB, Latham TE, Agans KN, Xu R, Ota-Setlik A, Egan MA, Fenton KA, Clarke DK, Eldridge JH, Geisbert TW. 2015. Single-dose attenuated Vesiculovax vaccines protect primates against Ebola Makona virus. *Nature* 520:688–691. <https://doi.org/10.1038/nature14428>.
- Bishnoi S, Tiwari R, Gupta S, Byrareddy SN, Nayak D. 2018. Oncotargeting by vesicular stomatitis virus (VSV): advances in cancer therapy. *Viruses* 10:90. <https://doi.org/10.3390/v10020090>.
- Stojdl DF, Lichty B, Knowles S, Marius R, Atkins H, Sonenberg N, Bell JC. 2000. Exploiting tumor-specific defects in the interferon pathway with a previously unknown oncolytic virus. *Nat Med* 6:821–825. <https://doi.org/10.1038/77558>.
- Stojdl DF, Lichty BD, tenOever BR, Paterson JM, Power AT, Knowles S, Marius R, Reynard J, Poliquin L, Atkins H, Brown EG, Durbin RK, Durbin JE, Hiscott J, Bell JC. 2003. VSV strains with defects in their ability to shut down innate immunity are potent systemic anti-cancer agents. *Cancer Cell* 4:263–275. [https://doi.org/10.1016/S1535-6108\(03\)00241-1](https://doi.org/10.1016/S1535-6108(03)00241-1).
- Westcott MM, Liu J, Rajani K, D'Agostino R, Lyles DS, Porosnicu M. 2015. Interferon beta and interferon alpha 2a differentially protect head and neck cancer cells from vesicular stomatitis virus-induced oncolysis. *J Virol* 89:7944–7954. <https://doi.org/10.1128/JVI.00757-15>.
- Rihn SJ, Aziz MA, Stewart DG, Hughes J, Turnbull ML, Varela M, Sugrue E, Herd CS, Stanifer M, Sinkins SP, Palmarini M, Wilson SJ. 2019. TRIM69 inhibits vesicular stomatitis Indiana virus (VISV). *bioRxiv* <https://doi.org/10.1101/669176>.
- Feng J, Wickenhagen A, Turnbull ML, Rezelj VV, Kreher F, Tilston-Lunel NL, Slack GS, Brennan B, Koudriakova E, Shaw AE, Rihn SJ, Rice CM, Bieniasz PD, Elliott RM, Shi X, Wilson SJ. 2018. Interferon-stimulated gene

- (ISG)-expression screening reveals the specific antibunyaviral activity of ISG20. *J Virol* 92:e02140-17. <https://doi.org/10.1128/JVI.02140-17>.
28. Whitt MA. 2010. Generation of VSV pseudotypes using recombinant DeltaG-VSV for studies on virus entry, identification of entry inhibitors, and immune responses to vaccines. *J Virol Methods* 169:365–374. <https://doi.org/10.1016/j.jviromet.2010.08.006>.
 29. Yap MW, Stoye JP. 2012. TRIM proteins and the innate immune response to viruses. *Adv Exp Med Biol* 770:93–104. https://doi.org/10.1007/978-1-4614-5398-7_7.
 30. Versteeg GA, Rajsbaum R, Sánchez-Aparicio MT, Maestre AM, Valdiviezo J, Shi M, Inn K-S, Fernandez-Sesma A, Jung J, García-Sastre A. 2013. The E3-ligase TRIM family of proteins regulates signaling pathways triggered by innate immune pattern-recognition receptors. *Immunity* 38:384–398. <https://doi.org/10.1016/j.immuni.2012.11.013>.
 31. Uchil PD, Hinz A, Siegel S, Coenen-Stass A, Pertel T, Luban J, Mothes W. 2013. TRIM protein-mediated regulation of inflammatory and innate immune signaling and its association with antiretroviral activity. *J Virol* 87:257–272. <https://doi.org/10.1128/JVI.01804-12>.
 32. Chawla-Sarkar M, Lindner DJ, Liu YF, Williams BR, Sen GC, Silverman RH, Borden EC. 2003. Apoptosis and interferons: role of interferon-stimulated genes as mediators of apoptosis. *Apoptosis* 8:237–249. <https://doi.org/10.1023/A:1023668705040>.
 33. Wang K, Zou C, Wang X, Huang C, Feng T, Pan W, Wu Q, Wang P, Dai J. 2018. Interferon-stimulated TRIM69 interrupts dengue virus replication by ubiquitinating viral nonstructural protein 3. *PLoS Pathog* 14: e1007287. <https://doi.org/10.1371/journal.ppat.1007287>.
 34. Kodama K, Doi O, Higashiyama M, Mori Y, Horai T, Tateishi R, Aoki Y, Misawa S. 1991. Establishment and characterization of a new Ewing's sarcoma cell line. *Cancer Genet Cytogenet* 57:19–30. [https://doi.org/10.1016/0165-4608\(91\)90185-W](https://doi.org/10.1016/0165-4608(91)90185-W).
 35. Stremlau M, Owens CM, Perron MJ, Kiessling M, Autissier P, Sodroski J. 2004. The cytoplasmic body component TRIM5alpha restricts HIV-1 infection in Old World monkeys. *Nature* 427:848–853. <https://doi.org/10.1038/nature02343>.
 36. Sudmant PH, Rausch T, Gardner EJ, Handsaker RE, Abyzov A, Huddleston J, Zhang Y, Ye K, Jun G, Fritz MH-Y, Konkel MK, Malhotra A, Stütz AM, Shi X, Casale FP, Chen J, Hormozdiari F, Dayama G, Chen K, Malig M, Chaisson MJP, Walter K, Meiers S, Kashin S, Garrison E, Auton A, Lam HYK, Mu XJ, Alkan C, Antaki D, Bae T, Cerveira E, Chines P, Chong Z, Clarke L, Dal E, Ding L, Emery S, Fan X, Gujral M, Kahveci F, Kidd JM, Kong Y, Lamejir E-W, McCarthy S, Flicke P, Gibbs RA, Marth G, Mason CE, Menelaou A, Muzny DM, Nelson BJ, et al. 2015. An integrated map of structural variation in 2,504 human genomes. *Nature* 526:75–81. <https://doi.org/10.1038/nature15394>.
 37. Marriott AC, Hornsey CA. 2011. Reverse genetics system for Chandipura virus: tagging the viral matrix protein with green fluorescent protein. *Virus Res* 160:166–172. <https://doi.org/10.1016/j.virusres.2011.06.007>.
 38. Sawyer SL, Wu LI, Emerman M, Malik HS. 2005. Positive selection of primate TRIM5α identifies a critical species-specific retroviral restriction domain. *Proc Natl Acad Sci U S A* 102:2832–2837. <https://doi.org/10.1073/pnas.0409853102>.
 39. Kumar S, Stecher G, Suleski M, Hedges SB. 2017. TimeTree: a resource for timelines, timetrees, and divergence times. *Mol Biol Evol* 34:1812–1819. <https://doi.org/10.1093/molbev/msx116>.
 40. Yang Z. 2007. PAML 4: phylogenetic analysis by maximum likelihood. *Mol Biol Evol* 24:1586–1591. <https://doi.org/10.1093/molbev/msm088>.
 41. Soll SJ, Wilson SJ, Kutluay SB, Hatzioannou T, Bieniasz PD. 2013. Assisted evolution enables HIV-1 to overcome a high TRIM5α-imposed genetic barrier to rhesus macaque tropism. *PLoS Pathog* 9:e1003667. <https://doi.org/10.1371/journal.ppat.1003667>.
 42. Rihn SJ, Foster TL, Busnadiego I, Aziz MA, Hughes J, Neil SJD, Wilson SJ. 2017. The envelope gene of transmitted HIV-1 resists a late interferon gamma-induced block. *J Virol* 91:e02254-16. <https://doi.org/10.1128/JVI.02254-16>.
 43. Busnadiego I, Kane M, Rihn SJ, Preugschas HF, Hughes J, Blanco-Melo D, Strouville VP, Zang TM, Willett BJ, Boutell C, Bieniasz PD, Wilson SJ. 2014. Host and viral determinants of Mx2 antiretroviral activity. *J Virol* 88:7738–7752. <https://doi.org/10.1128/JVI.00214-14>.
 44. Chandran K, Sullivan NJ, Felbor U, Whelan SP, Cunningham JM. 2005. Endosomal proteolysis of the Ebola virus glycoprotein is necessary for infection. *Science* 308:1643–1645. <https://doi.org/10.1126/science.1110656>.
 45. Novella IS, Clarke DK, Quer J, Duarte EA, Lee CH, Weaver SC, Elena SF, Moya A, Domingo E, Holland JJ. 1995. Extreme fitness differences in mammalian and insect hosts after continuous replication of vesicular stomatitis virus in sandfly cells. *J Virol* 69:6805–6809.
 46. Adams J, Kauffman M. 2004. Development of the proteasome inhibitor Velcade (Bortezomib). *Cancer Invest* 22:304–311. <https://doi.org/10.1081/CNV-120030218>.
 47. Dabiri Y, Kalman S, Gurth CM, Kim JY, Mayer V, Cheng X. 2017. The essential role of TAp73 in bortezomib-induced apoptosis in p53-deficient colorectal cancer cells. *Sci Rep* 7:5423. <https://doi.org/10.1038/s41598-017-05813-z>.
 48. Quintas-Cardama A, Vaddi K, Liu P, Manshoury T, Li J, Scherle PA, Caulder E, Wen X, Li Y, Waeltz P, Rupar M, Burn T, Lo Y, Kelley J, Covington M, Shepard S, Rodgers JD, Haley P, Kantarjian H, Fridman JS, Verstovsek S. 2010. Preclinical characterization of the selective JAK1/2 inhibitor INCB018424: therapeutic implications for the treatment of myeloproliferative neoplasms. *Blood* 115:3109–3117. <https://doi.org/10.1182/blood-2009-04-214957>.
 49. Everett RD, Rechter S, Papior P, Tavalai N, Stamminger T, Orr A. 2006. PML contributes to a cellular mechanism of repression of herpes simplex virus type 1 infection that is inactivated by ICPO. *J Virol* 80:7995–8005. <https://doi.org/10.1128/JVI.00734-06>.
 50. McEwan WA, Tam JC, Watkinson RE, Bidgood SR, Mallery DL, James LC. 2013. Intracellular antibody-bound pathogens stimulate immune signaling via the Fc receptor TRIM21. *Nat Immunol* 14:327–336. <https://doi.org/10.1038/ni.2548>.
 51. Pertel T, Hausmann S, Morger D, Züger S, Guerra J, Lascano J, Reinhard C, Santoni FA, Uchil PD, Chatel L, Bisiaux A, Albert ML, Strambio-De-Castillia C, Mothes W, Pizzato M, Grütter MG, Luban J. 2011. TRIM5 is an innate immune sensor for the retrovirus capsid lattice. *Nature* 472: 361–365. <https://doi.org/10.1038/nature09976>.
 52. Galao RP, Le Tortorec A, Pickering S, Kueck T, Neil SJ. 2012. Innate sensing of HIV-1 assembly by Tetherin induces NF-κB-dependent pro-inflammatory responses. *Cell Host Microbe* 12:633–644. <https://doi.org/10.1016/j.chom.2012.10.007>.
 53. Han Y, Li R, Gao J, Miao S, Wang L. 2012. Characterisation of human RING finger protein TRIM69, a novel testis E3 ubiquitin ligase and its subcellular localisation. *Biochem Biophys Res Commun* 429:6–11. <https://doi.org/10.1016/j.bbrc.2012.10.109>.
 54. Chen JL, Das T, Banerjee AK. 1997. Phosphorylated states of vesicular stomatitis virus P protein in vitro and in vivo. *Virology* 228:200–212. <https://doi.org/10.1006/viro.1996.8401>.
 55. Emerson SU, Schubert M. 1987. Location of the binding domains for the RNA polymerase L and the ribonucleocapsid template within different halves of the NS phosphoprotein of vesicular stomatitis virus. *Proc Natl Acad Sci U S A* 84:5655–5659. <https://doi.org/10.1073/pnas.84.16.5655>.
 56. Das T, Gupta AK, Sims PW, Gelfand CA, Jentoft JE, Banerjee AK. 1995. Role of cellular casein kinase II in the function of the phosphoprotein (P) subunit of RNA polymerase of vesicular stomatitis virus. *J Biol Chem* 270:24100–24107. <https://doi.org/10.1074/jbc.270.41.24100>.
 57. Gao Y, Lenard J. 1995. Multimerization and transcriptional activation of the phosphoprotein (P) of vesicular stomatitis virus by casein kinase-II. *EMBO J* 14:1240–1247. <https://doi.org/10.1002/j.1460-2075.1995.tb07107.x>.
 58. Gao Y, Lenard J. 1995. Cooperative binding of multimeric phosphoprotein (P) of vesicular stomatitis virus to polymerase (L) and template: pathways of assembly. *J Virol* 69:7718–7723.
 59. Spadafora D, Canter DM, Jackson RL, Perrault J. 1996. Constitutive phosphorylation of the vesicular stomatitis virus P protein modulates polymerase complex formation but is not essential for transcription or replication. *J Virol* 70:4538–4548.
 60. Barik S, Banerjee AK. 1992. Phosphorylation by cellular casein kinase II is essential for transcriptional activity of vesicular stomatitis virus phosphoprotein P. *Proc Natl Acad Sci U S A* 89:6570–6574. <https://doi.org/10.1073/pnas.89.14.6570>.
 61. Mondal A, Victor KG, Pudupakam RS, Lyons CE, Wertz GW. 2014. Newly identified phosphorylation site in the vesicular stomatitis virus P protein is required for viral RNA synthesis. *J Virol* 88:1461–1472. <https://doi.org/10.1128/JVI.02384-13>.
 62. Buchholz UJ, Finke S, Conzelmann KK. 1999. Generation of bovine respiratory syncytial virus (BRSV) from cDNA: BRSV NS2 is not essential for virus replication in tissue culture, and the human RSV leader region acts as a functional BRSV genome promoter. *J Virol* 73:251–259.
 63. Das SC, Baron MD, Skinner MA, Barrett T. 2000. Improved technique for transient expression and negative strand virus rescue using fowlpox T7 recombinant virus in mammalian cells. *J Virol Methods* 89:119–127. [https://doi.org/10.1016/S0166-0934\(00\)00210-X](https://doi.org/10.1016/S0166-0934(00)00210-X).

64. Wilson SJ, Schoggins JW, Zang T, Kutluay SB, Jouvenet N, Alim MA, Bitzegeio J, Rice CM, Bieniasz PD. 2012. Inhibition of HIV-1 particle assembly by 2',3'-cyclic-nucleotide 3'-phosphodiesterase. *Cell Host Microbe* 12:585–597. <https://doi.org/10.1016/j.chom.2012.08.012>.
65. Demaison C, Parsley K, Brouns G, Scherr M, Battmer K, Kinnon C, Grez M, Thrasher AJ. 2002. High-level transduction and gene expression in hematopoietic repopulating cells using a human immunodeficiency [correction of immunodeficiency] virus type 1-based lentiviral vector containing an internal spleen focus forming virus promoter. *Hum Gene Ther* 13:803–813. <https://doi.org/10.1089/10430340252898984>.
66. Kortekaas J, Oreshkova N, Cobos-Jimenez V, Vloet RP, Potgieter CA, Moormann RJ. 2011. Creation of a nonspreading Rift Valley fever virus. *J Virol* 85:12622–12630. <https://doi.org/10.1128/JVI.00841-11>.
67. Fukuyama S, Katsura H, Zhao D, Ozawa M, Ando T, Shoemaker JE, Ishikawa I, Yamada S, Neumann G, Watanabe S, Kitano H, Kawaoka Y. 2015. Multi-spectral fluorescent reporter influenza viruses (Color-flu) as powerful tools for in vivo studies. *Nat Commun* 6:6600. <https://doi.org/10.1038/ncomms7600>.
68. de Wit E, Spronken MI, Bestebroer TM, Rimmelzwaan GF, Osterhaus AD, Fouchier RA. 2004. Efficient generation and growth of influenza virus A/PR/8/34 from eight cDNA fragments. *Virus Res* 103:155–161. <https://doi.org/10.1016/j.virusres.2004.02.028>.
69. Dantuma NP, Lindsten K, Glas R, Jellne M, Masucci MG. 2000. Short-lived green fluorescent proteins for quantifying ubiquitin/proteasome-dependent proteolysis in living cells. *Nat Biotechnol* 18:538–543. <https://doi.org/10.1038/75406>.
70. Shalem O, Sanjana NE, Hartenian E, Shi X, Scott DA, Mikkelsen T, Heckl D, Ebert BL, Root DE, Doench JG, Zhang F. 2014. Genome-scale CRISPR-Cas9 knockout screening in human cells. *Science* 343:84–87. <https://doi.org/10.1126/science.1247005>.
71. Geoghegan V, Stainton K, Rainey SM, Ant TH, Dowle AA, Larson T, Hester S, Charles PD, Thomas B, Sinkins SP. 2017. Perturbed cholesterol and vesicular trafficking associated with dengue blocking in *Wolbachia*-infected *Aedes aegypti* cells. *Nat Commun* 8:526. <https://doi.org/10.1038/s41467-017-00610-8>.
72. Altschul SF, Madden TL, Schaffer AA, Zhang J, Zhang Z, Miller W, Lipman DJ. 1997. Gapped BLAST and PSI-BLAST: a new generation of protein database search programs. *Nucleic Acids Res* 25:3389–3402. <https://doi.org/10.1093/nar/25.17.3389>.
73. Nakamura T, Yamada KD, Tomii K, Katoh K. 2018. Parallelization of MAFFT for large-scale multiple sequence alignments. *Bioinformatics* 34:2490–2492. <https://doi.org/10.1093/bioinformatics/bty121>.
74. Suyama M, Torrents D, Bork P. 2006. PAL2NAL: robust conversion of protein sequence alignments into the corresponding codon alignments. *Nucleic Acids Res* 34:W609–W612. <https://doi.org/10.1093/nar/gkl315>.
75. Pond SL, Frost SD, Muse SV. 2005. HyPhy: hypothesis testing using phylogenies. *Bioinformatics* 21:676–679. <https://doi.org/10.1093/bioinformatics/bti079>.
76. Kosakovsky Pond SL, Posada D, Gravenor MB, Woelk CH, Frost SD. 2006. Automated phylogenetic detection of recombination using a genetic algorithm. *Mol Biol Evol* 23:1891–1901. <https://doi.org/10.1093/molbev/msl051>.
77. Crooks GE, Hon G, Chandonia JM, Brenner SE. 2004. WebLogo: a sequence logo generator. *Genome Res* 14:1188–1190. <https://doi.org/10.1101/gr.849004>.
78. Darriba D, Taboada GL, Doallo R, Posada D. 2012. jModelTest 2: more models, new heuristics and parallel computing. *Nat Methods* 9:772. <https://doi.org/10.1038/nmeth.2109>.
79. Guindon S, Dufayard JF, Lefort V, Anisimova M, Hordijk W, Gascuel O. 2010. New algorithms and methods to estimate maximum-likelihood phylogenies: assessing the performance of PhyML 3.0. *Syst Biol* 59:307–321. <https://doi.org/10.1093/sysbio/syq010>.
80. Walker PJ, Firth C, Widen SG, Blasdel KR, Guzman H, Wood TG, Paradkar PN, Holmes EC, Tesh RB, Vasilakis N. 2015. Evolution of genome size and complexity in the rhabdoviridae. *PLoS Pathog* 11:e1004664. <https://doi.org/10.1371/journal.ppat.1004664>.